Nano Research
2020, 13(7): 1795–1809

ISSN 1998-0124 CN 11-5974/O4
https://doi.org/10.1007/s12274-020-2661-8

Review Article

A mini-review on recent progress of new sensitizers for luminescence of lanthanide doped nanomaterials

Hongxin Zhang, Zi-Han Chen, Xuan Liu, and Fan Zhang (✉)

Department of Chemistry, Shanghai Key Laboratory of Molecular Catalysis and Innovative Materials, State Key Laboratory of Molecular Engineering of Polymers and iChem, Fudan University, Shanghai 200433, China

Received: 30 November 2019 / **Revised:** 13 January 2020 / **Accepted:** 14 January 2020

ABSTRACT

Trivalent lanthanide (Ln^{3+}) doped luminescent nanocrystals are promising for applications ranging from biosensor, lasing, super-resolution nanoscopy, information security and so on. Although the utility prospect is of great attractions, the light absorption of these lanthanide doped nanocrystals is inherently weak due to the electric dipole-forbidden 4f → 4f transitions. Even worse, the quantum yields of upconverison nanocrystals are very low, which will unavoidably hinder their further applications. In a typical lanthanide luminescent nanosystem, both sensitizers as light absorption centers and activators as light emitting centers are necessary and important for desired luminescence properties. Among various sensitization systems, only Yb^{3+} and Nd^{3+} are considered as the most efficient sensitizers. Thus, the corresponding excitation wavelengths are strictly limited around 980 and 808 nm. To enrich excitation wavelengths and boost luminescence intensity, exploring more sensitization units that possess larger absorption cross section, higher efficiency of energy transfer process and independent excitation is imperative and beneficial for the demands of different applications, such as broadened absorption in near infrared (NIR) region for higher conversion efficiency of solar cells, prolonged excitation wavelength to second near infrared windows region (NIR II, 1,000–1,700 nm) for *in vivo* fluorescence imaging with deeper tissue depth and higher spatial resolution, more orthogonal excitations and emissions to improve optical multiplexing, and so on. Therefore, in the review, we primarily conclude several major energy transfer mechanisms from sensitizers to activators. Then we present three kinds of sensitizers, including lanthanide ions, organic dyes and quantum dots (QDs), and introduce the newly designed sensitization system that allows us to exploit superior excitation wavelength and amplify luminescence intensity. Finally, several future challenges and opportunities for the sensitizing strategies are discussed in hope of directing and broadening the applications of lanthanide nanosystem.

KEYWORDS

lanthanide luminescence, new sensitizers, organic dyes, quantum dots

1 Introduction

Upconversion luminescence (anti-Stokes emissions) in trivalent lanthanide (Ln^{3+}) doped materials is a characteristic optical property [1–4]. The general concept of upconversion referring to a nonlinear optical progress through absorbing two or more lower energy photons and emitting one higher energy photon are first formulated independently by Auzel, Ovsyankin and Feofilov in the 1960s [1, 5]. However, the materials used for upconversion are usually limited to bulk form [6, 7]. Since the great development of nanotechnology [8, 9], Ln^{3+} doped upconversion nanocrystals with rational design of core/shell structures have drawn tremendous attentions due to their unique optical properties, including sharp-band emissions, excellent optical stability, low toxicity as well as long fluorescence lifetime [10–12]. Benefiting from the above merits, lanthanide doped luminescent materials emerging as new kinds of light emitters exhibit great potential applications on high-resolution nanoscopy [13, 14], optogenetics [15], lasing [16, 17], solar cell [18] and so on. Besides the upconversion behavior of Ln^{3+} doped nanomaterials, downshifting luminescence (Stokes emissions) of these nanocrystals in near infrared (NIR) region, especially in the wavelength range from 1,000 to 1,700 nm (NIR II window), also shows excellent superiority in the applications of bioimaging [19–21] and biosensing [22, 23].

Generally, upconversion and downshifting luminescence of most Ln^{3+} ions can be easily achieved through introducing suitable sensitizers that can efficiently absorb excitation photon energy and sequentially transfer energy to activators. Over the past decade, various lanthanide sensitizers, including Yb^{3+} (980 nm) [24], Nd^{3+} (808 nm) [25, 26], Er^{3+} (1,530, 808, and 980 nm) [27–29], Tm^{3+} (808, 1,064, and 1,208 nm) [20, 30, 31] and Ce^{3+} (254–450 nm) [32, 33], are developed to enrich the excitation wavelength and broaden their application, especially on biosensing [34], information storage [35] and lasing [16]. Among these sensitizers, only 980 nm excited Yb^{3+}-Ln^{3+} and 808 nm excited Nd^{3+}-Yb^{3+}-Ln^{3+} combinations are considered as the most efficient sensitization systems. Such limited sensitizers and corresponding excitation wavelengths are mainly caused by the fact that unlike the flexible absorption and structure of organic dyes and QDs, feature absorptions of lanthanide ions are fixed due to the unchanged excited states, and cross relaxation (CR) at high doping concentration is deleterious for both sensitizing and emitting processes, which will certainly result in the relatively

Address correspondence to zhang_fan@fudan.edu.cn

monotonous excitation wavelengths and sensitizers. More recently, researchers have demonstrated that organic dyes [36–38] and QDs [39–41], both of which show high absorption cross-section and abundant excitation wavelengths, emerge as new signposts to guide wider excitation wavelength range and stronger fluorescence intensity for lanthanide doped nanomaterials (Fig. 1).

In the view of recently extensive reports on Ln^{3+} doped nanocrystals, we mainly focus on the progress of newly developed sensitizers for upconversion and downshifting luminescence of Ln^{3+} doped nanoparticles. Different sensitizers for lanthanide luminescence involve in disparate mechanisms, thus we first illustrate several major energy transfer pathways from sensitizers to activators. Then we present a series of sensitizers, including lanthanide ions, organic dyes and QDs (Fig. 2), to induce lanthanide luminescence. In particular, we discuss the newly designed sensitization system that allows us to exploit superior excitation wavelengths and boost luminescence intensity for the applications on biosensing, information storage and lasing. Finally, several future challenges and opportunities for the sensitizing strategies are discussed in hope of directing and broadening the applications of functionalized lanthanide nanosystem.

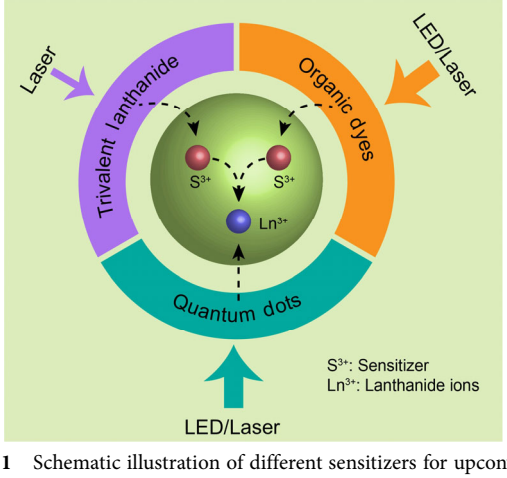

Figure 1 Schematic illustration of different sensitizers for upconversion and downshifting luminescence of lanthanide doped nanomaterials.

2 Energy transfer mechanisms for sensitizing lanthanide luminescence

Lots of studies are conducted to determine the energy transfer pathways of lanthanide luminescent nanosystem [37, 42–46]. Although higher sensitizer concentration may favor more excellent light absorption, the high doping could unavoidably cause localized concentration quenching of sensitizers or activators [29, 47]. So, to increase the light harvesting ability of Ln^{3+} doped nanomaterials, a sensitizer with larger absorption cross section is top priority. Besides, energy transfer efficiency that mainly depends on spectral overlap and distance between sensitizers and activators is another key factor that influences fluorescence intensity [48–50]. To optimize the luminescence performance of lanthanide doped nanocrystals, deep understandings on the intricate interactions between sensitizers and excitation source, sensitizers and activators, activators and activators are urgently needed. Therefore, we conclude several major sensitization mechanisms for lanthanide luminescence.

Upconversion in rare earth doped nanocrystals is an anti-Stokes and multi-photon process, in which excitation energy is transferred stepwise from sensitizers to activators [2, 3, 51]. The ladder-like electronic states of many Ln^{3+} ions and long radiative lifetimes (10 μs–10 ms) [10, 11, 52] of intermediate energy levels promote that upconverting process usually possesses as much as 10^6-fold higher efficiency than multi-photon absorption [53]. In host lattice, photon-assisted resonance energy transfer from sensitizers (Yb^{3+}) to activators (Fig. 3(a)), usually named as ETU, is highly effective, which greatly

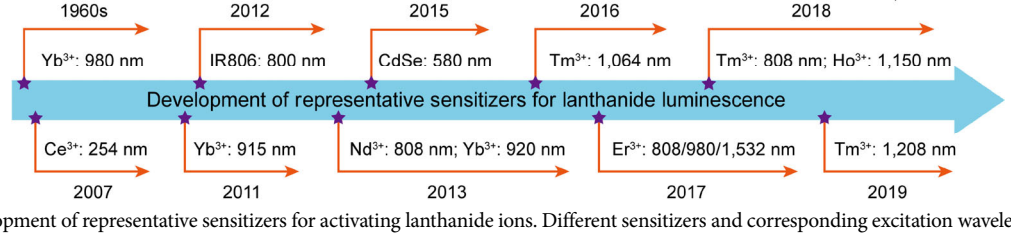

Figure 2 Development of representative sensitizers for activating lanthanide ions. Different sensitizers and corresponding excitation wavelength are provided.

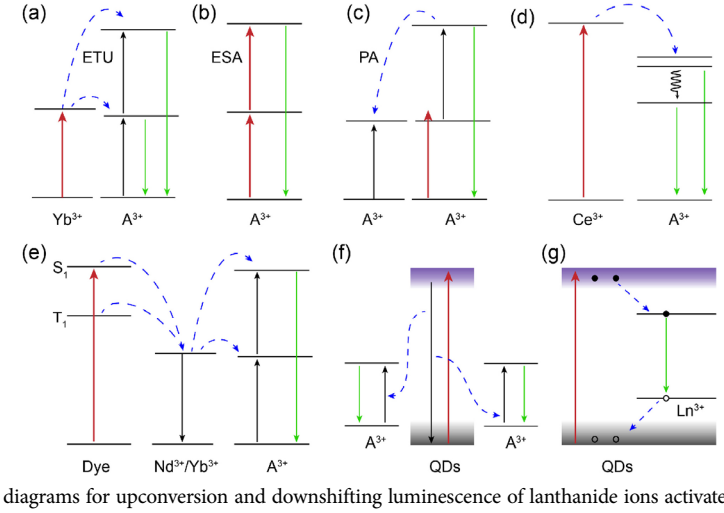

Figure 3 Simplified energy level diagrams for upconversion and downshifting luminescence of lanthanide ions activated by different sensitizers (lanthanide ions, dyes and quantum dots) through typical energy transfer pathways, including (a) energy transfer upconversion (ETU), (b) excited state absorption (ESA), (c) photon avalanche (PA), resonant energy transfer from (d) Ce^{3+} to Ln^{3+}, (e) dyes to Ln^{3+} and (f) quantum dots to Ln^{3+}, and (g) the energy transfer channel based on Ln^{3+} charge-transfer excited states.

contributes to the upconversion and downshifting luminescence of UCNPs [1]. In the case of excited state absorption (ESA), upconversion luminescence requires successive absorption of excitation photons by only one ion (Fig. 3(b)), in which only Er^{3+} doped nanoparticles are the usually reported nanosystems for efficient ESA process [46]. Photon avalanche (PA) induced upconversion (Fig. 3(c)) features an unusual luminescence mechanism that needs excitation power density to be above a certain threshold. Utilizing the PA process, researchers have successfully achieved extraordinary excitation wavelengths for the modulation of upconversion behavior on the applications of bioimaging [54], lasers [16] and super-resolution nanoscopy [13, 55]. For a long time, Ce^{3+} featuring broadband absorption in blue region (250–450 nm) due to the advantage of the parity-allowed 4f → 5d electronic transition has already been used as an efficient sensitizer for both downshifting and quantum cutting of lanthanide ions through resonant energy transfer (Fig. 3(d)) [33, 56–59]. However, the mechanism of energy transfer from Ce^{3+} to Ln^{3+} is still in debate about whether a charge-transfer of Ce^{4+}-Ln^{2+} is involved in the energy transfer that induces downshifting or downconversion luminescence [33].

Due to the forbidden nature of f–f transitions of Ln^{3+}, the absorption cross sections of Ln^{3+} ions are very small. Differently, small molecular dyes with controllable absorption peaks by modulating conjugated system have strong broadband absorption. Recently, scientists have demonstrated an effective method to amplify the absorption of lanthanide doped nanocrystals through anchoring organic dyes on their surface to implement an antenna effect. After light irradiation, the dyes around nanocrystals are activated to their excited singlet state, followed by two ways to activate lanthanide ions (Fig. 3(e)): (i) direct energy transfer from S_1 of dyes to sensitizers or activators on the surface of Ln^{3+} doped nanocrystals, or (ii) energy transfer from T_1 that originates from S_1 through intersystem crossing to sensitizers. Then the sensitizers in the nanocrystals will activate emitters by classical ETU mechanism for lanthanide luminescence [38, 60]. Since a pioneering concept proposed in 2012 by Jan C. Hummelen and co-workers [36], dye-sensitized structures for lanthanide luminescence have attracted enormous attentions and made great progress on various applications [60–63]. More importantly, the broadband sensitization from organic dyes indeed brings about enhanced luminescence intensity of Ln^{3+} doped nanocrystals even under incoherent light excitation [60]. However, every coin has two sides. Although the strategy shows impressive luminescence properties, the photobleaching of small molecule dye remains a big unfavorable obstacle for their practical applications [48]. Another problem is that until now the excitation wavelengths of most organic dyes for sensitizing Ln^{3+} ions are still less than 1,000 nm, which shows deleterious light scattering that goes against *in vivo* fluorescence imaging at deep tissue depth [64, 65].

Another reported method is to introduce QDs into lanthanide nanosystem. As is well known, QDs with controllable band gap by modulating sizes, shapes and compositions have strong broadband absorption [66, 67]. Hence, to enhance the light harvesting ability of lanthanide doped nanomaterials, researchers have successfully realized the combination of QDs and lanthanide ions to obtain efficient energy transfer from QDs to Ln^{3+} [68–70]. Up to now, two main energy transfer mechanisms are proposed to clarify luminescence behavior of lanthanide doped QDs. The first one is quantum cutting (downconversion, Fig. 3(f)), in which one pump photon captured by quantum dots can create two emissive photons from Ln^{3+}. In this way, the photoluminescence quantum yields of these nanosystems, where all-inorganic cesium lead halide $CsPbX_3$ nanocrystals are most used as host materials, are usually well over 100% [71]. Another energy transfer process is Ln^{3+} charge-transfer excited states (Fig. 3(g)), in which a photo-induced charge carrier in nanocrystals is formally absorbed by Ln^{3+} to generate Ln^{2+}, followed by internal conversion to promote the population of emissive excited state. The above process is proposed for sensitizing Yb^{3+} emission in bulk InP crystals [68]. However, the efficiencies of the charge-transfer process between QDs and Ln^{3+} are still limited and the narrow absorption, toxicity and stability of perovskite host will also hinder their widespread use [40]. Moreover, due to the complex doping system, the exact energy transfer mechanisms for lanthanide luminescence sensitized by QDs are very difficult to determine, more in-depth investigations are required.

3 Progress on sensitizers for lanthanide luminescence

Exploiting more sensitization units with the advantages of larger absorption cross section, higher energy transfer efficiency and diverse excitation wavelengths is necessary and important to meet the demands for different applications, such as wider absorption in NIR region for higher conversion efficiency of solar cells [72], longer excitation wavelength for *in vivo* fluorescence imaging at deeper tissue depth [20], more pump wavelengths for orthogonal excitation to improve multiplexing [73, 74], and so on. However, one must admit that there are several challenges on the way to reach this goal. For example, undesirable energy loss from cross relaxation between activators and activators/sensitizers, synthesis difficulty in combining a QD and lanthanide ions into a single nanoparticle, larger absorption overlap between diverse sensitizers hard for independent excitation without cross-talk. Therefore, great efforts should be devoted to promoting the development of new sensitizers for lanthanide luminescence.

3.1 Lanthanide ions as sensitizers

Among various lanthanide sensitizers, Yb^{3+} with large absorption cross-section (10^{-20} cm^{-2} at around 980) and only a single excited state is usually regarded as one of the most efficient sensitizers for activating most Ln^{3+}, including Er^{3+}, Tm^{3+}, Ho^{3+} and so on (Fig. 4(a)) [75–78]. The luminescence mechanism reveals effective photon-assisted resonance energy transfer from Yb^{3+} to activators in fluoride host lattice ($NaYF_4$, $NaGdF_4$, $NaLuF_4$ …) [79–82]. Great efforts have been devoted to developing multifarious Yb^{3+} sensitized lanthanide doped nanoparticles with abundant optical properties to greatly expand their applications. However, it is worth pointing out that one nonnegligible limitation of the most commonly used Yb^{3+} sensitized nanocrystals is their physically excitation band centered at 980 nm, overlapping at the absorption peak of water molecules [25, 26, 47]. Therefore, the 980 nm excitation energy would be significantly attenuated while traversing biological samples, resulting in the reduced fluorescence intensity and limited penetration depth. Moreover, the concomitantly induced overheating caused by 980 nm irradiation is another serious problem for the application in bio-system.

To address the challenge, considerable researches have focused on engineering the excitation wavelength for Ln^{3+} doped nanomaterials. For example, since the absorption cross-section of Yb^{3+} is broad, He and co-workers demonstrated that the 915 nm laser excitation on $NaYbF_4$: Ln^{3+} nanocrystals was superior to the 980 nm laser excitation for deep tissue imaging due to the low absorption coefficient of water at 915 nm [83]. Their further imaging analysis confirmed the practicability of the 915/920 nm lasers serving as new promising excitation

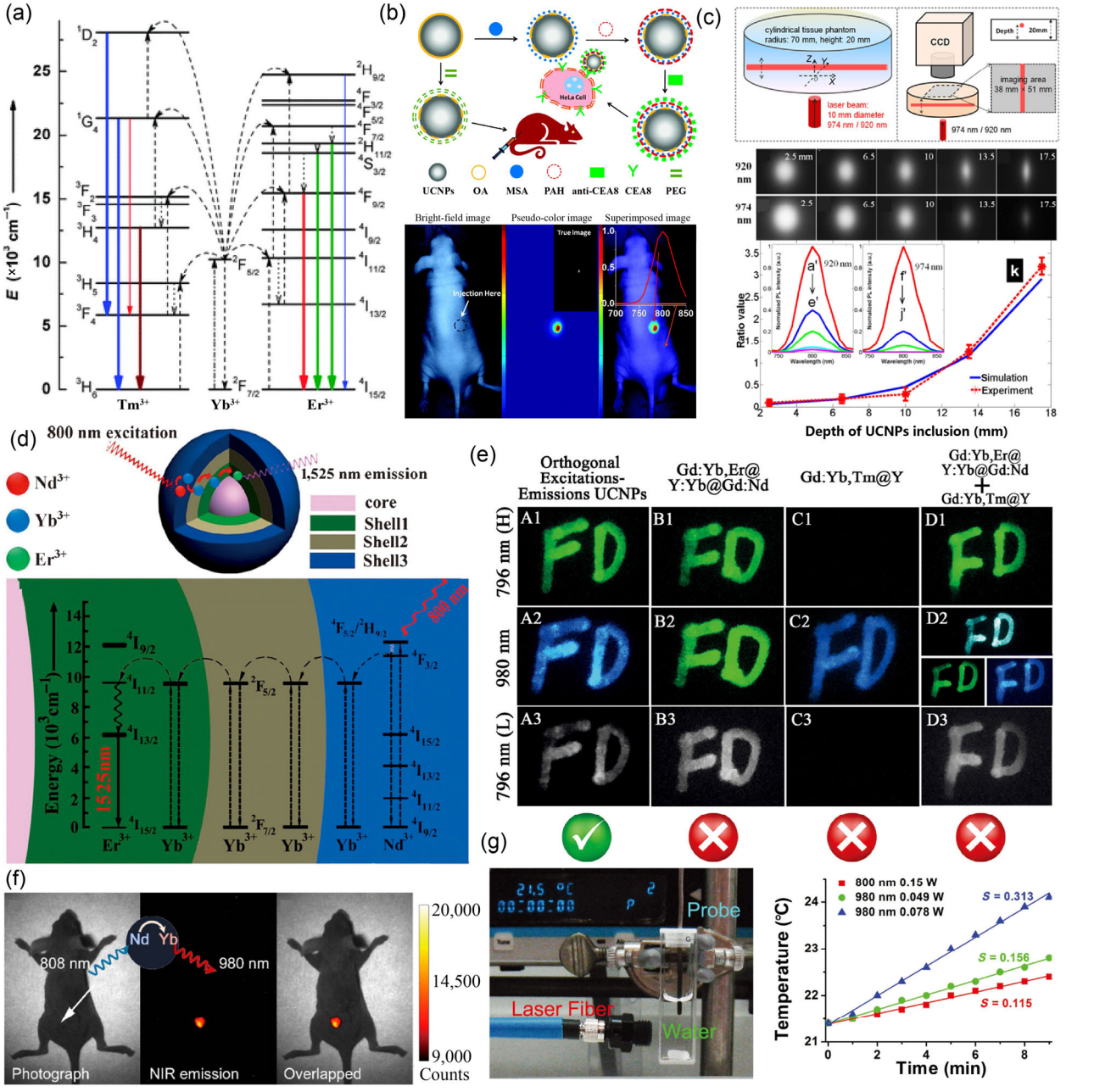

Figure 4 (a) Schematic energy level diagrams showing typical upconversion processes for Tm^{3+} and Er^{3+} sensitized by Yb^{3+} ion. (b) Schematic diagram illustrating bioconjugation process of OA-capped upconversion nanocrystals. Two pathways describe targeting HeLa cancer cell and *in vivo* animal imaging, respectively. The lower pictures show the *in vivo* imaging results based on $NaYbF_4$: Tm^{3+} nanocrystals excited by a 915 nm laser. (c) The set-up for comparison the penetration depth of 920 and 974 nm light for activating upconversion nanocrystals. The lower shows the experimental results indicating a deeper penetration of 920 nm light. (d) Proposed energy transfer mechanisms in the Nd^{3+} sensitized nanosystem. (e) Anti-counterfeiting luminescence images of the orthogonal excitations-emissions of different excitation wavelengths, emissions and nanocrystals. (f) *In vivo* fluorescence imaging of Nd^{3+} sensitized nanicrystals under an 808 nm laser excitation. (g) The experimental setup for evaluating heating effect of water under 980 and 800 nm lasers excitation. The results of the heating effect of lasers irradiation are on the right. 800 nm irradiation shows lower increase on temperature. Reproduced with permission from Ref. [83], © American Chemical Society 2011; Ref. [84], © Ivyspring International Publisher 2013; Ref. [94], © Wiley-VCH 2014; Ref. [73], © Wiley-VCH 2016; Ref. [25], © American Chemical Society 2013; and Ref. [26], © Wiley-VCH 2013.

lights for Yb^{3+}-sensitized nanomaterials (Figs. 4(b) and 4(c))) [84]. However, the absorption cross-sections of Yb^{3+} at 915/920 nm are very low, leading to the weak luminescence intensity compared to that excited by a 980 nm laser under the same power density. This will undoubtedly cause energy loss of excitation lasers and undesirably increase the energy flux irradiated on bio-samples, which is unamiable for bio-imaging and detection.

To further distance the excitation wavelength from absorption peak of water and meanwhile guarantee an acceptable light absorption of a sensitizer (Fig. 5(a)), one needs to be familiar with the typical absorption spectra of most lanthanide ions (Fig. 5(b)). Notably, Nd^{3+} has strong absorption peaks at wavelengths far from 980 nm, such as 740, 794, and 862 nm (Fig. 5(b)), assigned to the transitions from $^4I_{9/2}$ to $^4F_{7/2}$, $^4F_{5/2}$ and $^4F_{3/2}$, respectively. Importantly, all of these peaks (especially the absorption peak at 794 nm with the absorption cross section of about 10^{-19} cm^{-2}) are corresponding to the weak absorption of water. Utilizing the above property and valid energy transfer from Nd^{3+} to Yb^{3+} [85–87] in different host materials (up to 70%), a new assembly of Yb^{3+}/Nd^{3+}/Ln^{3+} cascade sensitized tri-doped nanoparticles under the excitation around

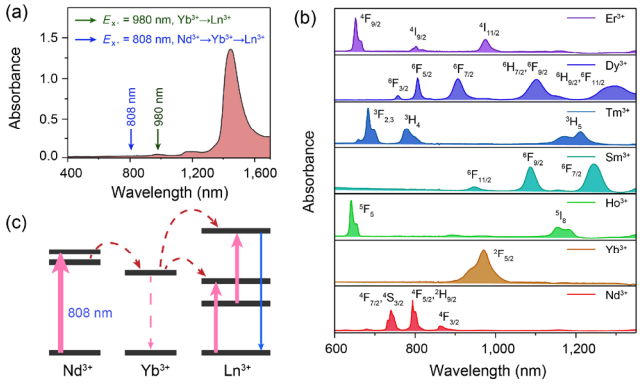

Figure 5 (a) Absorption spectrum of pure water through a cuvette with 1-mm width. (b) Absorption spectra of most lanthanides ions in aqueous solution (0.05 M). Other lanthanides, such as Pr^{3+}, Eu^{3+} and Tb^{3+}, show ignorable absorption intensity in the wavelength range from 600 to 1,350 nm. The width of cuvettes used here are 1 cm. (c) Simplified sensitization process of Nd^{3+}/Yb^{3+} co-doped system under an 808 nm laser excitation.

800 nm are proposed (Fig. 5(c)), in which Nd^{3+} ions take the role of absorbing pump photons, while the Yb^{3+} ions act as bridging ions to further transfer energy to activators [87, 88]. However, this tri-doped nanostructure allows only for low concentration doping of Nd^{3+} ions, resulting in feeble absorption and thus weak emission intensity. Although the higher concentration of Nd^{3+} would favor better absorption, the high doping could unavoidably cause deleterious cross relaxation between Nd^{3+} ions and emitters, which will consume most of the pump energy. Therefore, the early Nd^{3+} sensitized upconversion nanocrystals excited by an 800 nm laser is relatively weak compared to that of Yb^{3+}-based counterparts upon a 980 nm laser excitation. The relevant investigation on these tri-doping structures mainly focuses on the optical properties and energy transfer mechanism.

Until 2013, several group teams independently proposed a rational core/shell structures, including $NaYF_4$:Yb^{3+}/Nd^{3+}/Ln^{3+}@$NaYF_4$:Nd^{3+} [47], $NaGdF_4$:Yb^{3+}/Ln^{3+}@$NaGdF_4$:Nd^{3+}/Yb^{3+} [25] and $NaGdF_4$:Nd^{3+}@$NaGdF_4$:Yb^{3+}/Ln^{3+} [89], to separate the activators and Nd^{3+} and thus increase the doping concentration of sensitizers for the sake of more excellent light absorption and reduced energy loss from ions interactions (Fig. 4(d)). The luminescence intensity of the above Nd^{3+}-sensitized core/shell nanocrystals is dramatically enhanced by the factor of about 405 compared to that achievable using the nanocrystals without the high doping shell coating of Nd^{3+} [47]. Soon after, benefiting from the drastically enhanced luminescence intensity of Nd^{3+}-sensitized core/shell structures under a 808 nm laser excitation, various applications including anti-counterfeiting (Fig. 4(e)) [90], therapy [91, 92], bio-detection [93], bio-imaging (Fig. 4(f)) [94] and color modulation [95, 96] of lanthanide doped nanomaterials are greatly enriched and improved. For example, our group designed core–multishell structured $NaGdF_4$:Yb, Er@$NaYF_4$:Yb@$NaGdF_4$:Yb,Nd@$NaYF_4$@$NaGdF_4$:Yb,Tm@$NaYF_4$ nanoparticles with power-density independent orthogonal excitations-emissions upconversion luminescence and demonstrated their potential application on multi-dimensional security marking (patterns, emissions and excitations) and imaging-guided combined therapy [73]. The most important thing is that the heating effect of 800 nm irradiation is lower than that of 980 nm (Fig. 4(g)). However, Nd^{3+}-based nanostructures usually needs the assistance of Yb^{3+} ions as bridging role for efficient sensitization, which will certainly require the complicated and niggling core/shell designs for eagerly awaited applications.

Besides Yb^{3+} and Nd^{3+}, Er^{3+} possesses excellent sensitization efficiency as well. In 2017, three groups independently found an efficient core-inert shell nanostructure with a strongly suppressed concentration quenching effect of Er^{3+} in core area (Fig. 6(a)) [27–29], for which the optimized doping concentration of Er^{3+} can reach up to 100%. The important inert shell of $NaYF_4$ acts as a perfect protecting layer to prevent energy migration to the surface of nanocrystals. In such luminescence system, Er^{3+} ions serve as both sensitizers and activators by ESA and ETU, in which 808, 980, and 1,530 nm lasers are all favorable excitation sources. The quantum yield of Er^{3+} self-sensitized upconversion nanocrystals (0.17%) is comparable to conversional Yb^{3+} sensitized upconversion nanocrystals under excitation with a 980 nm diode laser [28]. It should be noted that the construction of pure Er^{3+}-based host sensitization nanocrystals only offers the ability to generate bright red emission, while the featured green emission at 525 and 540 nm of Er^{3+} are nearly blocked due to the CR at high doping concentration of Er^{3+} [45]. Taking advantage of the unique optical property, tunable full color emission in a single core-shell structured nanocrystal by three continuous wave (CW) lasers [76] and image-guided photoinduced "off–on" therapy in biomedicine (Fig. 6(b)) [34] are both achieved.

Apart from self-sensitization, Er^{3+} can also activate other Ln^{3+} ions. For example, Huang developed a brand-new design of upconversion nanocrystals, where the typically less than 10% doped Er^{3+} ions were used to transfer the absorbed photon energy at 1,532 nm to nearby lanthanide emitters for their upconversion luminescence, including Nd^{3+}, Eu^{3+}, Ho^{3+}, and Tm^{3+} [35]. Resonant energy transfer mechanism was proposed to be responsible for the Er^{3+} sensitized nanosystem. Yb^{3+} with the excited state overlapping with the $^4I_{11/2}$ state of Er^{3+} could extract the energy of Er^{3+} and consequently modulate the emission properties of activators in the tri-doping (Er^{3+}-Yb^{3+}-Ln^{3+}) system. High-level anticounterfeiting was demonstrated through combining these nanocrystals with commonly used Yb^{3+}-sensitized ones. At the same time, our group also reported a series of Er^{3+} sensitized nanocrystals ($NaErF_4$:Ho^{3+}@$NaYF_4$ and $NaErF_4$@$NaYF_4$: Nd^{3+}@$NaYF_4$) with both excitation and emissions located in the NIR-II window (Fig. 6(c)) [22]. Based on the ratiometric fluorescence by combining the efficient NIR-II upconversion emissions and H_2O_2 sensing organic chromophore probe IR1061, the microneedle patch sensor (Fig. 6(d)) for *in vivo* inflammation dynamic detection was developed (Fig. 6(e)). Subsequently, similar Er^{3+}-sensitized results were further confirmed by Zhang and coworkers [45]. Developments up to now, although Er^{3+} ions as both sensitizers and emitters show excellent luminescence intensity of upconverison and downshifting, the luminescence intensities of other activators sensitized by Er^{3+} are relatively low due to the inefficient energy transfer efficiencies from Er^{3+} to activators as well as the deleterious CR between Er^{3+} and activators. Further studies on fine doping and core/shell nanostructures are still required in the future.

Alternatively, Tm^{3+} is also reported as a newly developed sensitizer. Two decent absorption peaks around 800 and 1,200 nm (Fig. 5(b)) provide the possibility of designed energy transfer process from Tm^{3+} to activators. Jia introduced the blue upconversion luminescence of only Tm^{3+} doped $NaYF_4$ nanocrystals under an 800 nm laser excitation through ground state absorption (GSA) and ESA, in which the luminescence intensity would be sharply amplified after incorporating bridging ions Yb^{3+} into the nanocrystals while keeping the excitation wavelength at 800 nm [31]. The mechanism of the enhanced luminescence intensity was demonstrated that electron energy on the $^3H_4$ state of Tm^{3+} could be transferred to the $^2F_{5/2}$ state of Yb^{3+} through multi-phonon assisted process, followed by the efficient back energy transfer from Yb^{3+} to Tm^{3+}. However, the

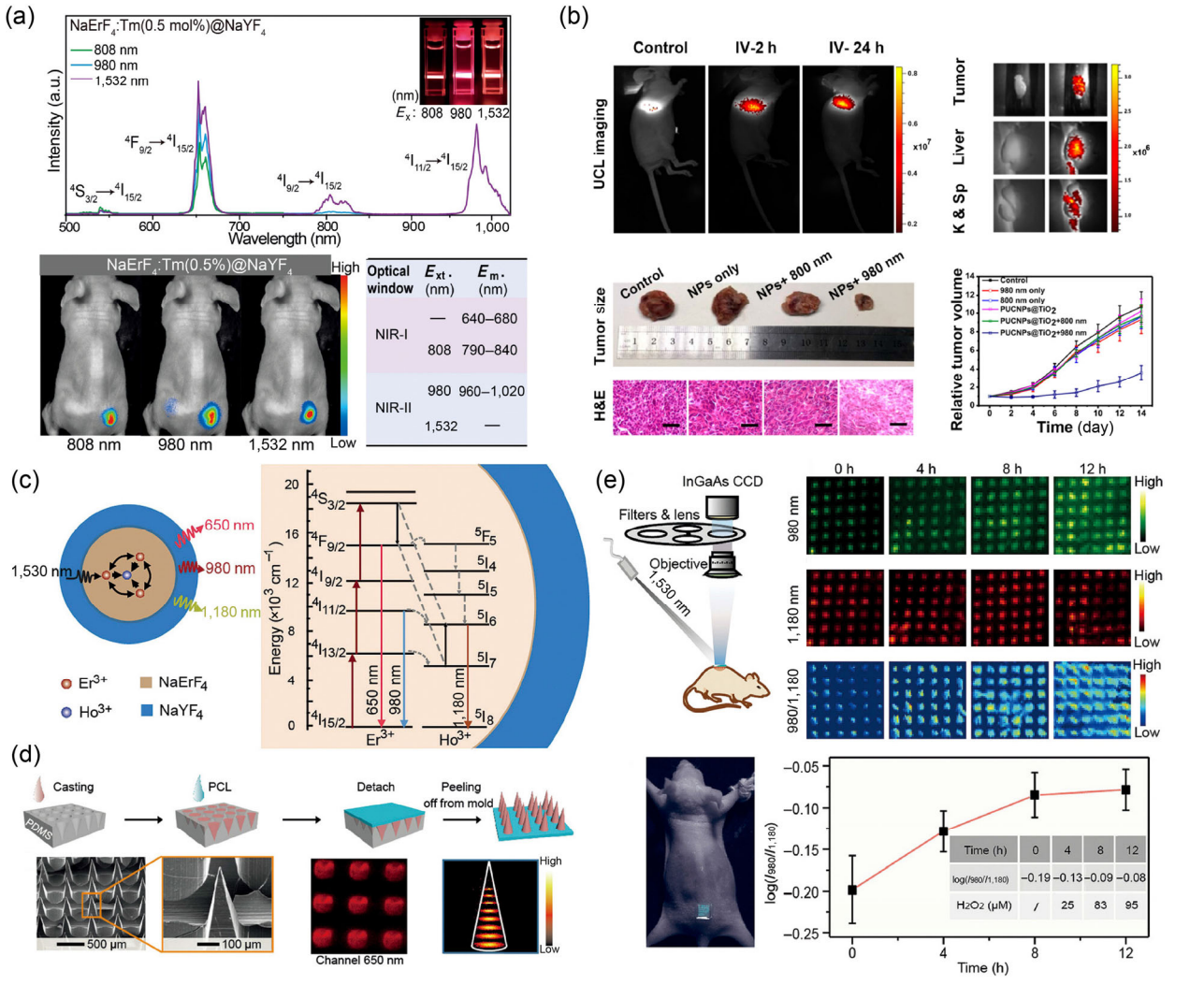

Figure 6 (a) Emission spectra of highly Er^{3+} doped nanocrystals NaErF:0.5%Tm^{3+}@$NaYF_4$ excited by 808, 980 and 1,532 nm lasers. The lower pictures are results of *in vivo* fluorescence imaging. (b) The highly Er^{3+} doped nanocrystals are used for imaging-guided tumor therapy. (c) Schematic illustration of Er^{3+} sensitized photon upconversion under 1,532 nm excitation. The proposed energy transfer pathway from Er^{3+} to Ho^{3+} is also shown here. (d) The fabrication process, SEM and confocal laser scanning microscopy images of the microneedle patch. (e) The *in vivo* bioimaging experimental setup and results of *in vivo* detection on H_2O_2 concentration at different time. Reproduced with permission from Ref. [28], © Wiley-VCH 2017; Ref. [34], © American Chemical Society 2018; and Ref. [22], © Wiley-VCH 2018.

relevant studies on these nanostructures are still confined to spectral measurements due to their weaker emission intensities than that of conversional Yb^{3+} sensitized nanocrystals, which implies that such Tm^{3+} sensitization system under an 800 nm laser excitation is still far from practical application.

Sometimes, weak GSA but strong ESA process of one identical excitation wavelength under higher power density can also induce considerable upconversion luminescence, usually named as PA process. Based on this upconversion mechanism, the only Tm^{3+} doped nanocrystals excited at 1,064 nm can emit upconverted luminescence at 800 nm (Fig. 7(a)) [54]. In the design, the small GSA of 1,064 nm occurs through the high energy tail or phonon sideband of the Tm^{3+}: $^3H_6 \rightarrow {}^3H_5$ transition centered at 1,200 nm. Then the electron energy on $^3F_4$ state relaxed from $^3H_5$ undergoes the efficient ESA1: $^3F_4 \rightarrow {}^3F_{2,3}$ transition at 1,064 nm. Two CR processes, including $^3H_4 + {}^3H_6 \rightarrow 2\ {}^3F_4$ and $^3H_4 + {}^3F_4 \rightarrow 2\ {}^3H_5 \rightsquigarrow 2\ {}^3F_4$, further induce the energy population of $^3F_4$ state. After most Tm^{3+} ions are excited to the intermediate state $^3F_4$, the efficiency of ESA1 will be indisputably promoted to amplify the population of $^3F_{2,3}$ state, followed by the non-radiative relaxation process: $^3F_{2,3} \rightsquigarrow {}^3H_4$, thus emitting strong upconversion fluorescence at 800 nm (Figs. 7(a) and 7(b)). The calculated quantum yield of 8 nm nanocrystals doped with 1% Tm^{3+} is estimated to be 0.046%. Although the utilities of the only Tm^{3+} doped nanocrystals for cell imaging (Fig. 7(c)) and micro-lasing (Fig. 7(d)) [16] were demonstrated, one should notice that the energy looping process is only observed at high excitation flux larger than 3×10^3 W/cm^2 in a confocal microscope, which is difficult for large scale *in vivo* fluorescence imaging.

The Tm^{3+} sensitized upconversion process can also be applied to Ho^{3+} activator through resonant energy transfer from Tm^{3+} to Ho^{3+} and a subsequent ESA process of Ho^{3+} under an 808 nm laser excitation ((Fig. 7(e)). Taking advantage of the efficient energy transfer process, Carvajal demonstrated that $KLu(WO_4)_2$: Ho^{3+},Tm^{3+} nanoparticles were able to combine controllable heat release and upconversion thermometry permitting to estimate its thermal resistance in air [30]. Recently, our group found that Tm^{3+} could also activate upconversion and downshifting luminescence of Er^{3+} in codoped nanocrystals excited by a 1,208 nm laser [20]. The quantum yield of the downshifted emission at 1,525 nm could reach up to 0.22%, which was sufficient for the application on *in vivo* information storage and decoding with high spatial resolution and large optical multiplexed capacity (Fig. 7(f)). However, in this Tm^{3+} sensitization system, the upconversion luminescence in visible range

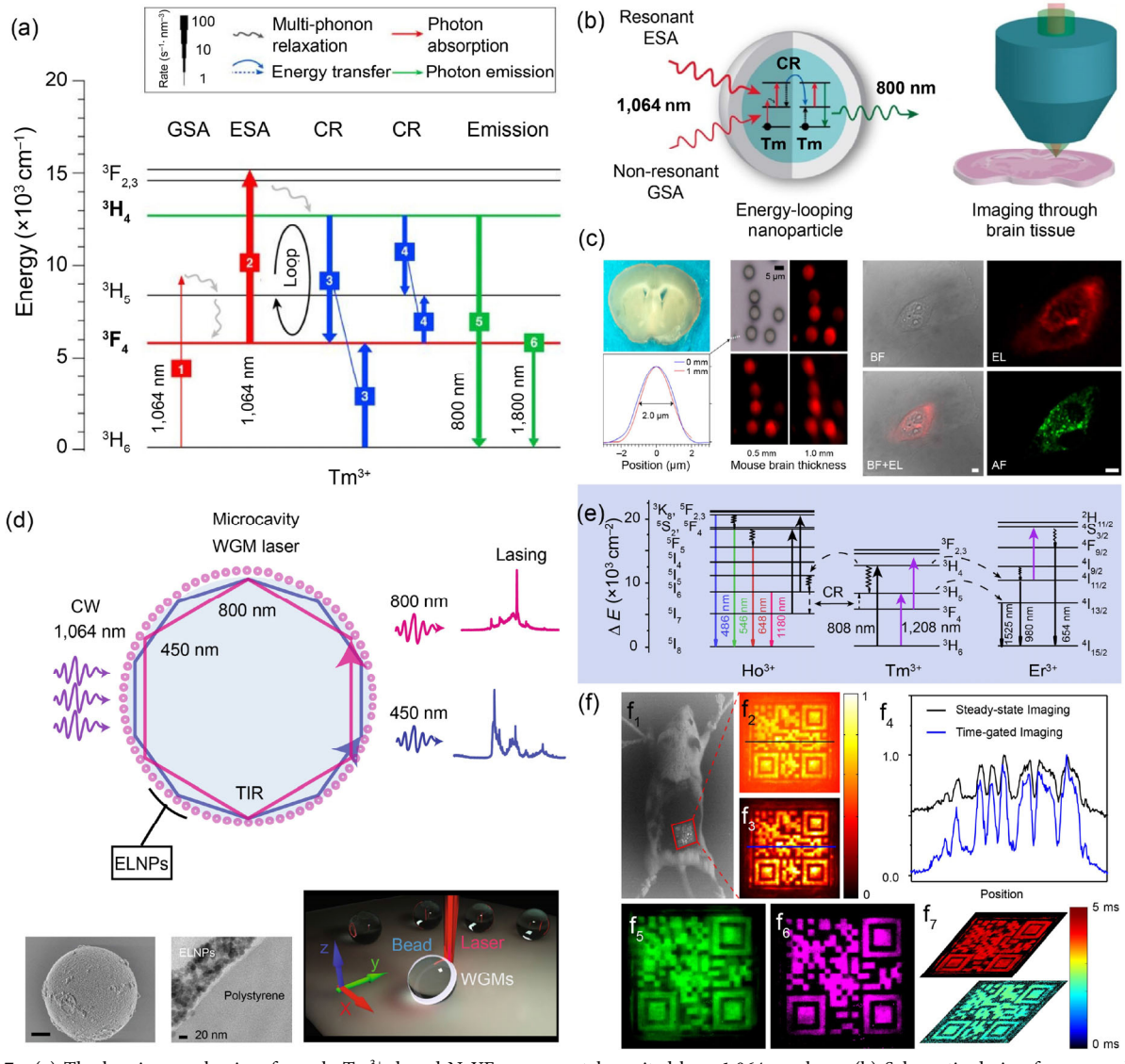

Figure 7 (a) The looping mechanism for only Tm^{3+} doped $NaYF_4$ nanocrystals excited by a 1,064 nm laser. (b) Schematic design for energy-looping nanocrystals for imaging through brain tissue. (c) The Tm^{3+} doped nanocrystals are loaded into microbeads, which are located underneath a mouse brain slice with different thickness (0.5 and 1 mm). The results indicate a good optical penetration of the bio-sample. Confocal imaging of live HeLa cell after treatment with Tm^{3+} doped nanocrystals. (d) Schematic of excitation and lasing in $NaYF_4$:Tm^{3+}-coated microbeads. TEM images are on the left bottom. (e) The energy transfer channels from Tm^{3+} to Ho^{3+} and Er^{3+}. (f) *In vivo* fluorescence imaging at 1,525 nm. f_2, f_3 and f_4 indicate the high signal to noise imaging by using time-gated imaging system. f_5 and f_6 show the QR code image with longer fluorescence lifetime. f_7 is the fluorescence lifetime images. Reproduced with permission from Ref. [54], © American Chemical Society 2016; Ref. [16], © Springer Nature 2018; and Ref. [20],© Wiley-VCH 2019.

is only spectrally measurable but hard for actual use.

Interestingly, lanthanide ion Ho^{3+}, a common activator with green and red emissions, could also serve as a sensitizer to populate its high excited states through GSA and ESA when excited by an 1,150 nm laser [97]. With Er^{3+} codoping, the characteristic peaks of Er^{3+} at 525, 550, and 658 nm appeared obviously, straightforwardly suggesting the role of Ho^{3+} as a sensitizer to activate the emissions of Er^{3+}.

As is well known, because of the electric dipole-allowed 4f → 5d transition, Ce^{3+} characterized broadband absorption from 250 to 450 nm has already been served as an efficient sensitizer for both downshifting and downconversion luminescence of Ln^{3+}. In 2013, Jang achieved highly bright multicolor-emitting $Na(Y/Gd)F_4$:Ce/Tb/Eu@$NaYF_4$ nanocrystals with the particle size less than 10 nm and quantum yield of 1.1%–6.9%, to which a hand-held ultraviolet lamp (λ = 254 nm) rather than a laser was applied [57]. Gd^{3+} in the host plays an important role in enhancing emission intensity of Eu^{3+} and Tb^{3+} through the more efficient energy transfer pathway: Ce^{3+}→Gd^{3+}→Ln^{3+}. When Nd^{3+} ions were used as emitters, downconversion of one ultraviolet excitation photon occurred, resulting in one visible photon and one NIR photon (Fig. 8(a)) [33]. After integrated into a c-Si solar cell, the downconversion nanocrystals contribute to a 1.2-fold enhancement in short-circuit current (Fig. 8(b)). As a new independent excitation and energy transfer channel, dual excitation and emission in a core-shell nanostructure could be easily constructed for anticounterfeiting application (Fig. 8(c)), in combination with upconversion ones [58, 98]. Recently, scientists have demonstrated the superiority of NIR II fluorescence probes for bioimaging with high spatial resolution and tissue penetration [99–101]. With this background, Chen designed NIR II luminescence nanocrystals based on efficient energy transfer from Ce^{3+} to Er^{3+} (E_m.: 1,525 nm) and Nd^{3+} (E_m.: 1,060 nm) in CaS nanocrystals with the Stokes shift near 1,100 nm (Fig. 8(d)) [32]. Although Ce^{3+} sensitization provides an alternative way for downshifting and downconversion luminescence of Ln^{3+} with high quantum yields compared to those of upconversion process (Table 1), the excitation source with the wavelength located from 250 to 450 nm is harmful and not very suitable for bio-samples.

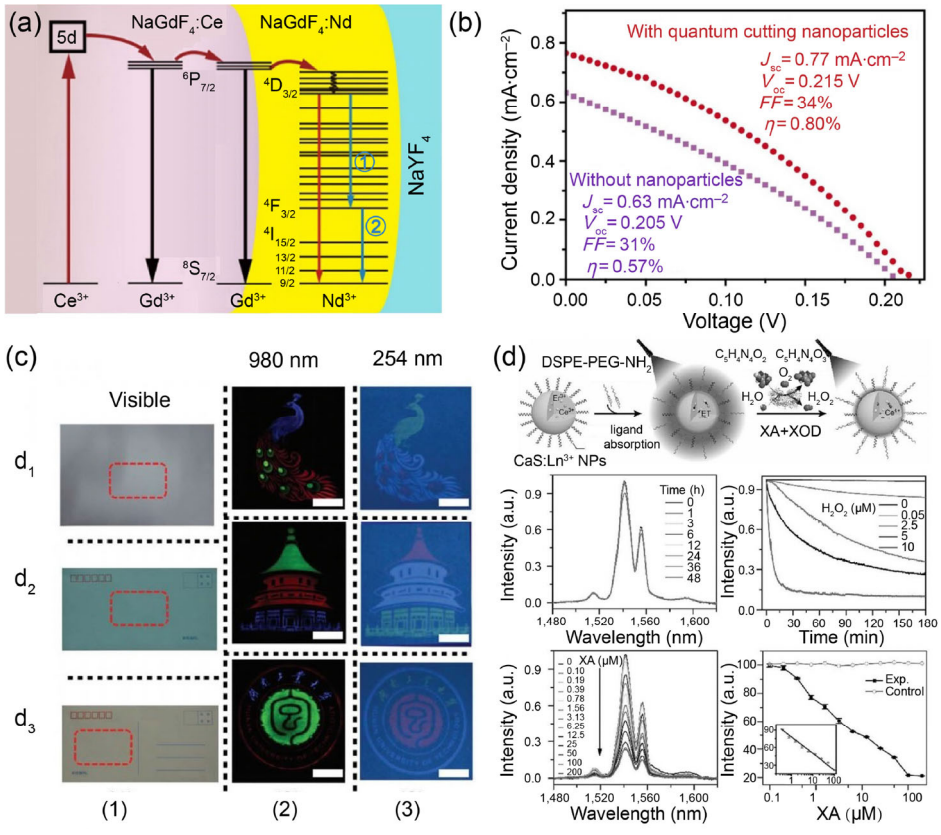

Figure 8 (a) Schematic energy transfer for the Ce^{3+} sensitized quantum cutting in Nd^{3+} ions. (b) The current density–voltage performance for c-Si solar cells with and without nanocrystals coating layer. The samples were irradiated by a 254 nm UV lamp (7 mW/cm^2). (c) Using dual excitation and emission properties of a core-shell nanostructure based on Ce^{3+} and Yb^{3+} sensitization system, anticounterfeiting application is confirmed. A 980 nm laser and a 254 nm UV lamp are used. (d) Schematic for the detection of XA through XA/XOD enzymatic reaction based on Lipo-coated CaS: Ce^{3+}, Er^{3+} nanoprobes. Reproduced with permission from Ref. [33], © American Chemical Society 2017; Ref. [98], © The Royal Society of Chemistry 2019; and Ref. [32], © Wiley-VCH 2019.

Table 1 Summary of lanthanide ions to sensitize the upconversion and downshifting luminescence of lanthanide activators

Excitation wavelength (nm)	Sensitizer	Activators	Nanocrystals	Applications	Refs.
980/915/920 (laser)	Yb^{3+}	Er^{3+}, Tm^{3+}, Ho^{3+}…	$NaYF_4$:Yb^{3+}/Ln^{3+}, $NaYbF_4$: Ln^{3+}, $NaYF_4$:Yb^{3+}/Er^{3+}	Live cell membrane imaging, *in vivo* bio imaging …	[5, 83, 84]
808/795/740 (laser)	Nd^{3+}	Er^{3+}, Tm^{3+}, Ho^{3+}…	$NaYF_4$:Yb^{3+}/Nd^{3+}/Ln^{3+}@$NaYF_4$:Nd^{3+}, $NaGdF_4$:Yb^{3+}/Ln^{3+}@$NaGdF_4$:Nd^{3+}/Yb^{3+}, $NaGdF_4$:Nd^{3+}@$NaGdF_4$:Tm^{3+}/Yb^{3+}	*In vivo* bioimaging, imaging-guided combined photodynamic therapy …	[25, 47, 89]
808/980/1,530 (laser)	Er^{3+}	Er^{3+}, Ho^{3+}, Nd^{3+}, Yb^{3+}, Eu^{3+}, Tm^{3+}…	$NaErF_4$@$NaYF_4$, $NaErF_4$:Tm^{3+}@$NaYF_4$, $NaErF_4$:Ho^{3+}@$NaYF_4$, $NaErF_4$@$NaYF_4$:Nd^{3+}@$NaYF_4$, $NaYF_4$:Er^{3+}/Nd^{3+}, $NaYF_4$:Er^{3+}/Tm^{3+}/Yb^{3+}, $NaYF_4$:Er^{3+}/Ho^{3+}/Yb^{3+}	Anticounterfeiting, *in vivo* biosensing and imaging …	[22, 27–29, 35, 45]
808/1,208 (laser)	Tm^{3+}	Er^{3+}, Ho^{3+}, Yb^{3+}…	$NaYF_4$:Er^{3+}/Tm^{3+}@$NaYF_4$, $NaHoF_4$:Tm^{3+}@$NaYF_4$, $NaYF_4$:Yb^{3+}/Tm^{3+}@$NaYF_4$, $KLu(WO_4)_2$:Ho^{3+}/Tm^{3+}	*In vivo* informayion storage and decoding, thermometry …	[20, 30]
1,150 (laser)	Ho^{3+}	Er^{3+}, Ho^{3+}…	$NaYF_4$:Ho^{3+}, $NaYF_4$:Ho^{3+}/Er^{3+}	—	[35]
254–450 (UV lamp)	Ce^{3+}	Eu^{3+}, Er^{3+}, Nd^{3+}, Gd^{3+}, Tb^{3+}…	$Na(Y/Gd)F_4$:Ce/Tb/Eu@$NaYF_4$, $NaYF_4$:Yb^{3+}/Ln^{3+}@$NaGdF_4$:Ce^{3+}/Ln^{3+}, CaS:Ce^{3+}/Ln^{3+}, $NaGdF_4$:Ce^{3+}@$NaGdF_4$:Nd^{3+}@$NaYF_4$	Anti-counterfeiting, multicolor display, pH sensing, solar cells …	[32, 33, 57, 58, 98]

3.2 Organic dyes as sensitizers

To break the bottleneck of the inherently weak and narrowband absorption of lanthanide ions, small molecule organic dyes with large absorption cross section (10^{-17}–10^{-16} cm^2) are employed as antenna to enhance the quantum yields and brightness of upconversion nanocrystals. The seminal demonstration on the dye sensitization concept was reported in 2012 (Fig. 9(a)), where the extinction coefficient of the named dye IR-806 at 806 nm was about 5 × 10^6 times higher than that of $NaYF_4$: Yb^{3+}/Er^{3+} nanocrystals at 975 nm [36]. The quantum yield of the IR-806/nanocrystals was determined as 0.12%, slightly less than that of the non-sensitized oleylamine-coated nanocrystals (0.3%). Considering the excellent absorption cross section of the antenna IR-806, the broad spectral response in the 720–1,000 nm range from the dye-coated nanocrystals was 3,300 times higher than that of the non-dye-sensitized system. After that, a series of dye-sensitized upconversion nanocrystals with distinctive absorption ranges were developed to boost lanthanide luminescence intensity.

However, because most of the excitation wavelengths of the antennas are located around 800 nm (Table 2), the energy transfer efficiency from organic dyes to Yb^{3+} with the maximal absorption around 980 nm is not optimal. Therefore, to further

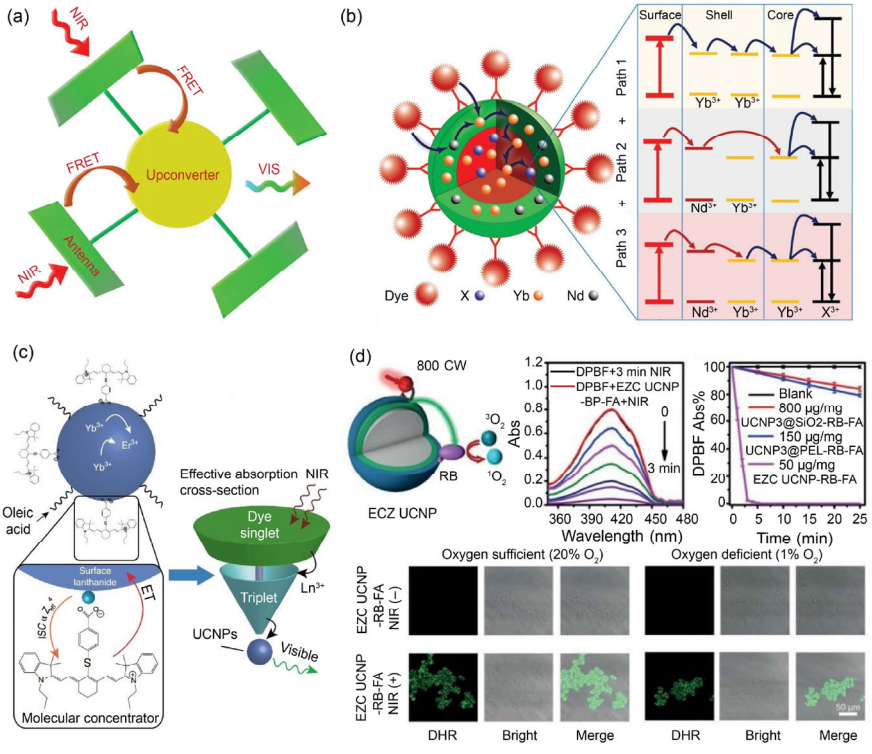

Figure 9 (a) Green boxes represent the antenna dyes that absorbs near infrared light (red wavy arrows), and then the energy is transferred to the nanocrystal core (in yellow) by FRET, inducing upconversion luminescence. (b) Three different energy cascaded pathways for dye-sensitized upconversion luminescence are proposed. ICG is used as an antenna. Nd^{3+} and Yb^{3+} ions are doped in the outer shell to enhance energy transfer efficiency from antenna to lanthanides. (c) Schematic illustration of IR806 sensitized upconversion process. Heavy lanthanide ions, such as Gd^{3+}, can promote intersystem crossing to enhance population of triplet stats, boosting the energy transfer efficiency from organic dyes to lanthanide ions. (d) The ROS generation process is shown in the top left. The changes of absorbance of DPBF under near infrared excitation for 3 min and of DPBF in 50 μg/mL ECZ UCNP-RB-FA dispersion under near infrared excitation for 0 to 3 min. Confocal microscopic images of HeLa cells after incubation using DHR for 30 min, and then 50 μg/mL ECZ UCNPs-RB-FA under O_2-sufficient and O_2-deficient microenvironment for 6 h under near infrared excitation for 5 min. Reproduced with permission from Ref. [36], © Macmillan Publishers Limited 2012; Ref. [50], © Wiley-VCH 2016; Ref. [42], © Macmillan Publishers Limited, part of Springer Nature 2018; and Ref. [102], © Wiley-VCH 2019.

Table 2 Summary of representative organic dyes to sensitize the upconversion and downshifting luminescence of lanthanide activators

Excitation wavelength (nm)	Sensitizer	Nanocrystals	Applications	Refs.
808 (laser)	Cy787	$NaYF_4$: Yb^{3+}/Nd^{3+}/Er^{3+}@$NaYF_4$: Nd^{3+}	Detection of ClO^-	[104]
808 (laser)	IRDye 800CW	$NaYF_4$:Gd^{3+}@$NaYF_4$:Yb^{3+}/Er^{3+}@$NaYF_4$:Nd^{3+}/Yb^{3+}	Detection of Hg^{2+} and photodynamic therapy	[102]
808 (laser)	IR808	$NaGdF_4$:Yb^{3+}/Er^{3+}@$NaGdF_4$:Yb^{3+}	Detection of intracellular ClO^-	[103]
808 (laser)	Cynn	$NaYF_4$:Yb^{3+}/Er^{3+}@$NaYF_4$:Nd^{3+}	Detection of phosgene	[105]
808 (laser)	IR806	$NaLuF_4$:Gd^{3+}/Yb^{3+}/Er^{3+}@$NaYF_4$ (or $NaGdF_4$)	—	[42]
808 (laser)	Cy-GSH	$NaYF_4$:Yb^{3+}/Er^{3+}@$NaYF_4$:Nd^{3+}	GSH imaging	[106]
980 (laser)	IR1061	$NaYF_4$:Yb^{3+}/Tm^{3+}@$NaYF_4$:Yb^{3+}	—	[63]
800 (laser)	ICG	$NaYF_4$: Yb^{3+}/Er^{3+}@$NaYbF_4$@$NaYF_4$:Nd^{3+}	NIR-II region deep optical imaging	[107]
800 (laser)	BODIPY-FL, Cy3.5, IR806	$NaYF_4$:Yb^{3+}/Tm^{3+}	Information security technology	[108]
800 (laser)	IR806	$NaYF_4$:Yb^{3+}/Er^{3+}@$NaYF_4$:Yb^{3+}	Photodynamic therapy and bioimaging	[109]
800 (laser)	ICG	$NaYF_4$: Yb^{3+}/X^{3+}@$NaYF_4$: Yb^{3+} (X = Er, Tm and Ho)	Photographic images	[50]
800 (laser)	IR808	$NaYbF_4$:Tm^{3+}@$NaYF_4$:Nd^{3+}	—	[60]

improve the spectral overlap between organic dyes and Ln^{3+}, Nd^{3+} sensitized nanocrystals with the superior absorption at 800 nm are applied. Combining the Nd^{3+} doped core/shell nanostructures $NaYF_4$:Yb^{3+}/X^{3+}@$NaYF_4$:Yb^{3+}/Nd^{3+} with ICG dye, the upconversion luminescence intensity was enhanced by a factor of 2 ~ 3 compared to that of ICG sensitized and only Yb^{3+} doped nanocrystals $NaYF_4$:Yb^{3+}/X^{3+}@$NaYF_4$:Yb^{3+} (Fig. 9(b)) [50]. As a deeper mechanism investigation, Garfield et al. revealed that heavy lanthanides, such as Gd^{3+}, could facilitate the population of triplet state of dye antennas, resulting in the enhanced energy transfer efficiency and amplified luminescence brightness of dye-sensitized upconversion nanocrystals (Fig. 9(c)) [42].

Besides the doping compositions, the architectures of the upconversion nanocrystals can also affect the energy transfer efficiency from dyes to Ln^{3+}. Through subsequently coating emitting layer ($NaYF_4$: Yb^{3+}/Er^{3+}) and energy absorption layer ($NaYF_4$:Nd^{3+}/Yb^{3+}) with antenna 800CW on the surface of an inert core ($NaYF_4$: Gd), the upconversion luminescence was

enhanced by 2 times due to the shrunken distance between sensitizers and activators [102]. Another important merit owe to the easily functionalized organic dyes is that the dye-sensitized upconversion nanosystem is favorably able to be designed for targeted bio-sensing based on responsive antennas (Fig. 9(d)) [102–104]. Despite these efforts [105–109], some obstacles and limitations of the dye-sensitized design, such as low spectral overlap between antennas and lanthanide sensitizers, energy dissipation of lanthanide sensitizers, the low photostability of organic dyes, and relatively confined excitation wavelength shorter than 1,000 nm for commercially available dyes, remain big challenges.

3.3 QDs as sensitizers

Doping lanthanide with QDs is a prospering research field (Table 3). As early as 2002, Klik et. al reported the energy transfer mechanism responsible for the Ln^{3+} luminescence in semiconductor [68]. The lanthanide ions doping introduces isoelectronic acceptor-like trap into host. These related traps would capture electrons or holes generated from semiconductor band-to-band excitation and binding with corresponding carriers by Coulomb potential induced charge compensation. Then the non-radiative recombination of these electron-hole pairs from the trap leads to the excitation of lanthanide ions. Over the past decade, spectral properties of lanthanides (Tb^{3+}, Eu^{3+} and Yb^{3+}) in various semiconductor nanoparticles host matrix have been investigated, including ZnS [110], CdSe [69, 111] and $PbIn_2S_4$ (Fig. 10(a)) [112]. These studies combine strong ultraviolet/visible broadband absorption with the sharp lanthanide emission opens up a possibility of novel nano-

Table 3 Summary of representative QDs to activate lanthanide luminescence

Excitation wavelength (nm)	Sensitizer	Lanthanide component	Applications	Refs.
808 (laser)	Ag_2Se	$NaYF_4$:Yb^{3+}/Gd^{3+}/Er^{3+}@ $NaYF_4$:Nd^{3+}/sYb^{3+}	Photoluminescence and PDT efficiency	[41]
365 (light)	$CsPbCl_xBr_yI_{3-x-y}$	Yb^{3+}, Nd^{3+}, Dy^{3+}, Tb^{3+}, Pr^{3+}, Ce^{3+}	Solar cell application	[39]
375 (laser)	$CsPbCl_3$	Yb^{3+}	—	[71]
275 (xenon lamp)	$CsPbBr_3$	Eu^{3+}, Tb^{3+}	—	[113]
440 (laser)	InP@$LnYF_3$@ShF_3 (Sh = Lu, Y)	Yb^{3+}, Nd^{3+}	—	[40]
405 (laser)	$PbIn_2S_4$	Yb^{3+}	—	[112]
350/285 (unknown)	CdSe	Yb^{3+}, Tb^{3+}	—	[69, 111]

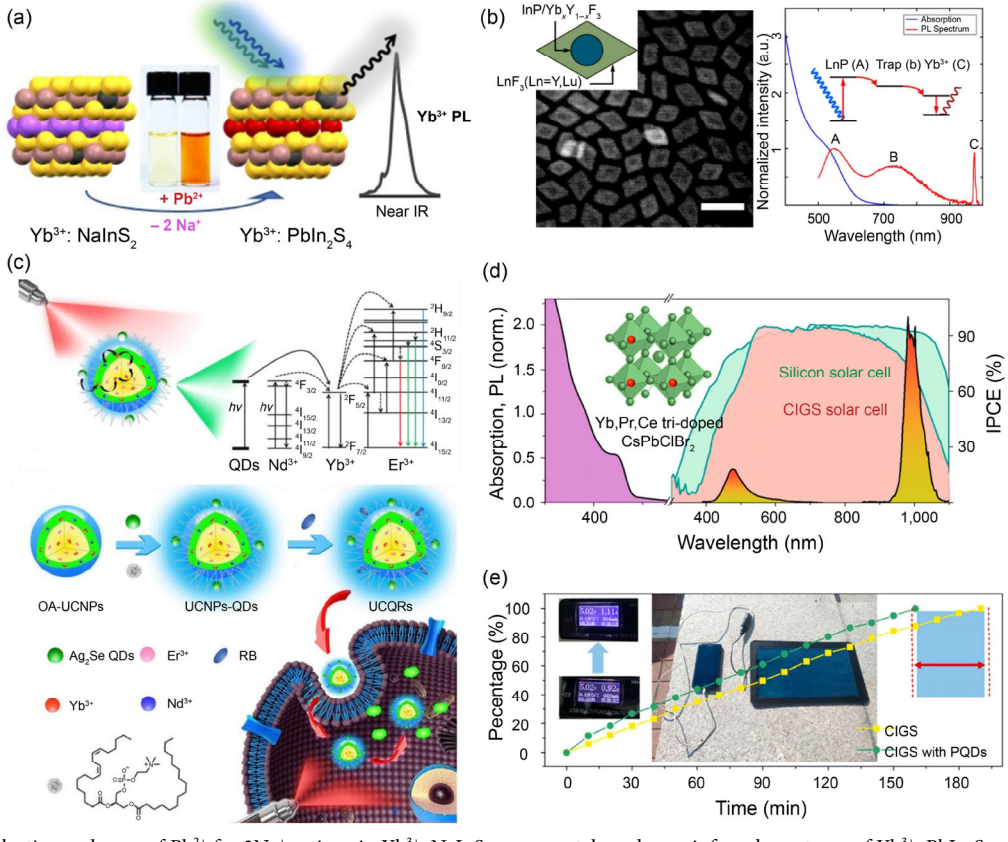

Figure 10 (a) Selective exchange of Pb^{2+} for $2Na^+$ cations in Yb^{3+}: $NaInS_2$ nanocrystals and near infrared spectrum of Yb^{3+}: $PbIn_2S_4$ nanocrystals under 405 nm excitation. (b) HAADF-STEM image of InP@$Y_{1-x}Yb_xF_3$@LuF_3 core/shell/shell nanocrystals. Absorption (blue) and photoluminescence (λ_{ex}= 440 nm) (red) of the core/shell/shell nanocrystals. Scale bar: 50 nm. (c) Schematic illustration (upper) of the energy transfer process in QDs sensitized Nd^{3+}/Yb^{3+} co-doped upconversion nanocomposites and upconversion nanocrystals-QDs (lower) combined with photosensitizers (Rose Bengal) for photodynamic therapy. (d) Absorption (purple) and photoluminescence (reddish yellow) spectra of Yb,Pr,Ce tri-doped $CsPbClBr_2$ QDs. The incident photon-to-current conversion efficiency curves of a silicon (green) and CIGS (red) solar cell coated with Yb^{3+}, Pr^{3+}, Ce^{3+} tri-doped $CsPbClBr_2$ PQDs. (e) Comparison of time for fully charging a mobile phone with a CIGS solar cell coated with Yb^{3+}, Pr^{3+}, Ce^{3+} tri-doped $CsPbClBr_2$ PQDs and a CIGS solar cell alone under the irradiation of sunlight. Inset: display of charging power and charging scene arrangement. Reproduced with permission from Ref. [112], © American Chemical Society 2017; Ref. [40], © American Chemical Society 2018; Ref. [41], © American Chemical Society 2019; and Ref. [39], © American Chemical Society 2019.

phosphor. However, due to a poor affinity of lanthanide ions and semiconductor lattices, incorporation of lanthanide is often unfavorable and results in less than 10% concentration of doping. The limited energy transfer efficiency reduces luminous efficiency, thus making it impractical in real application.

Alternatively, separation between lanthanides doped nanohosts and QDs hosts can also induce effectual energy transfer from QDs to rare earth ions. A. Paul Alivisatos reported the first synthesis of core/shell/shell InP@$Ln_xY_{1-x}F_3$@ShF_3 (Ln = Yb, Nd; Sh = Lu, Y) nanostructures that exhibited a broad visible absorption coupled to a sharp NIR emission (Fig. 10(b)) [40]. In the nanocrystals, InP QDs were used as a light absorber and $Ln_xY_{1-x}F_3$ acted as a light emitting layer, while the growing outer layer ShF_3 served as a passivating shell to prevent surface quenching. The photoluminescence quantum yield of 0.1%–0.5% remained low due to the reduced wave function overlap between the band-gap and the Yb-related trap state. The coupling may be improved in the future through materials selection and nanostructure tuning. Recently, Liu and co-workers reported a nano-composition through anchoring Ag_2Se quantum dots on the surface of $NaYF_4$:Yb^{3+}, Gd^{3+}, Er^{3+} nanocrystals to achieve the efficient upconversion luminescence by the energy transfer from QDs to Ln^{3+} under an 808 nm laser excitation (Fig. 10(c)) [41]. A better ability of the synthesized composite to induce cell apoptosis and inhibit tumor growth was confirmed, further demonstrating the promising potential of quantum dots for sensitizing lanthanide luminescence. Actually, the structural stability and uniformity of the assembled nanocomposite still need to be improved.

Halide perovskite $CsPbX_3$ QDs, emerging as a new class of nanomaterials, have attracted extensive interests due to their high photoluminescence quantum yields, broadband absorption, and band gap tunability throughout the ultraviolet, visible, and NIR spectrum via size control (the famous quantum size effect) and compositional alloying [71]. Recently, researchers have found that introduction of some rare earth ions with near-infrared emissions into lattices of halide perovskite QDs can exhibit the excellent optical properties of both Ln^{3+} ions and the perovskite QDs [113, 114]. The extremely efficient sensitization of Ln^{3+} luminescence in $CsPbX_3$ host performs over 100% yields through the lattice defect participated quantum cutting effect (Figs. 10(d) and 10(e)) [71]. Unfortunately, the toxic component of halide perovskite and instability for water and oxygen hinder the use in bio-application. Future research on coupling lanthanide with compatible host of sufficient conversion efficiency is still challenging and desirable.

4 Outlook and challenges

In this review, we surveyed and summarized recent progress on exploring more efficient and practical sensitizers for the upconversion and downshifting luminescence of lanthanide doped nanocrystals. Several energy transfer pathways from sensitizers to activators for lanthanide luminescence are systematically introduced. Three kinds of energy absorbents and donors, including Ln^{3+}, organic dyes and QDs, are discussed successively. Up to now, various sensitizers summarized in Tables 1–3 are developed to improve the luminescence performance and strengthen their practicability. Benefiting from the great efforts and contributions on the newly developed sensitization nanosystem, numerous applications, such as Tm^{3+} sensitized NIR II excitation and NIR II emission nanocrystals for *in vivo* fluorescence imaging and information decoding with deeper tissue penetration and higher spatial resolution [20], target-responsive dye to sensitize lanthanide luminescence for bio-detection [103] and *in vivo* imaging with higher accuracy and signal-to-background ratio [106], are further promoted.

Although various sensitization units are demonstrated, lots of problems and challenges still exist considering the real use of these newly developed sensitization system in near future. For lanthanide ions as sensitizers, except Yb^{3+} only having one excited state, most sensitizers reported now possess abundant energy levels, which will easily lead to multiple interactions between neighboring ions (CR process) that probably accompanied by energy loss of excitation photons. So, for different lanthanide sensitizers, correspondingly fine modulations on doping concentrations, lanthanide distributions and core/multi-shell nano-design to essentially enhance luminescence intensity of upconversion and downshifting are eagerly desired. Recently, scientists found that NIR II light showing little scattering when traversing bio-tissue is more suitable for bioimaging with higher resolution and penetration depth [65]. Apart from NIR II fluorescence, this principle is also appropriate for excitation source. When the NIR II lasers traverse bio-samples, the lower scattering of excitation source will induce a higher power density irradiating on the fluorescence probes at the deeper tissue depth. That is to say, brighter emissions will be obtained under NIR II lasers excitation. Actually, due to the absorption of water around 1,200 and 1,500 nm, the now reported NIR II excitation wavelengths (1,208 and 1,532 nm) are not the optimal ones for *in vivo* bioimaging. Further investigations on sensitizers, such as Dy^{3+} and Sm^{3+} ions both exhibiting intense absorption around 1,100 nm (Fig. 5(b)), to avoid water absorption of excitation source (wavelength range from 1,020 to 1,110 nm in Fig. 5(a)) are still on the way.

The dye-sensitized lanthanide luminescence has already been proposed for more than seven years, huge advancements on the nanosystem for applications of bio-detection and bioimaging have been witnessed. However, some challenges on this kind of sensitization system are still disturbing us. One is the photostability of organic dyes on the surface of lanthanide doped nanomaterials. Although the luminescence performance of dye-sensitized nanosystem is indeed improved, the measured quantum yields of these nanomaterials remain limited. For a brighter emission, the excitation power density will be increased inevitably to a higher level, which will cause serious photobleaching, especially for applications of cell imaging using microscope. So, further studies on designing more stable organic dyes as antennas to sensitize lanthanide are pressingly required. Another problem is about the energy transfer efficiency from dyes to lanthanides that needs to improve. The spectral overlap and physical distance between dyes and lanthanides are two main factors that will influence the sensitization efficiency. Engineering organic antennas and screening suitable lanthanides as well as reasonable core/shell nanostructures with larger spectral overlap and shortened donor-acceptor distance may be more advantageous to improve lanthanide luminescence in dye-sensitized nanosystem. Besides, the number of organic molecular anchored on the surface of one lanthanide doped nanocrystal can also affect the luminescence intensity. Because the over-concentrated dyes around nanocrystals will induce aggregation concentration quenching of organic dyes as well as back energy transfer from lanthanides to dyes, which is disadvantageous for lanthanides luminescence.

Lanthanide luminescence sensitized by QDs has reported for decades. However, upconversion behavior, one typical optical anti-Stokes property of Ln^{3+} doped nanocrystals, has not been reported so far [41]. The relative slow development on these nanomaterials is mainly due to the following problems. The first one is the general difficulty of incorporating Ln^{3+} in quantum dots lattices. Ln^{3+} ions often possess larger coordination numbers of six or greater, making incorporation at tetrahedral

lattice sites such as the common binary chalcogenide/pnictide semiconductors thermodynamically unfavorable. To mitigate the problem, various methods such as cation exchange, optimized QDs hosts, core/multi-shell structures and particles cross-linking are proposed to promote the combination of QDs and Ln^{3+} for the sake of better luminescence intensity. The second is bio-toxicity of QDs, which is a wheezy but important problem that hinders widespread expansion of QDs and scares away explorers. Certainly, the primary task for QDs sensitized lanthanide luminescence is to make the luminescence intensity strong enough for applications in the labs. Although Ln^{3+} doped halide perovskite shows high quantum yields, the narrowness of the absorption and stability of the perovshite host remain to be solved. Despite these challenges, we believe that breakthroughs on QDs sensitized lanthanide luminescence will be made in the future.

Acknowledgements

The work was supported by the National Key R&D program of China (No. 2017YFA0207303), the National Natural Science Foundation of China (Nos. 21725502 and 21701027), and Key Basic Research Program of Science and Technology Commission of Shanghai Municipality (No. 17JC1400100).

References

[1] Auzel, F. Upconversion and anti-Stokes processes with f and d ions in solids. *Chem. Rev.* **2004**, *104*, 139–173.

[2] Fan, Y.; Liu, L.; Zhang, F. Exploiting lanthanide-doped upconversion nanoparticles with core/shell structures. *Nano Today* **2019**, *25*, 68–84.

[3] Chen, X.; Peng, D. F.; Ju, Q.; Wang, F. Photon upconversion in core-shell nanoparticles. *Chem. Soc. Rev.* **2015**, *44*, 1318–1330.

[4] Li, X. M.; Zhang, F.; Zhao, D. Y. Lab on upconversion nanoparticles: Optical properties and applications engineering via designed nanostructure. *Chem. Soc. Rev.* **2015**, *44*, 1346–1378.

[5] Wang, F.; Liu, X. G. Recent advances in the chemistry of lanthanide-doped upconversion nanocrystals. *Chem. Soc. Rev.* **2009**, *38*, 976–989.

[6] Yeh, D. C.; Sibley, W. A.; Suscavage, M. J. Efficient frequency upconversion of Tm^{3+} ions in Yb^{3+} doped barium-thorium fluoride glass. *J. Appl. Phys.* **1988**, *63*, 4644–4650.

[7] Tanabe, S.; Yoshii, S.; Hirao, K.; Soga, N. Upconversion properties, multiphonon relaxation, and local environment of rare-earth ions in fluorophosphate glasses. *Phys. Rev. B* **1992**, *45*, 4620–4625.

[8] Wang, F.; Han, Y.; Lim, C. S.; Lu, Y. H.; Wang, J.; Xu, J.; Chen, H. Y.; Zhang, C.; Hong, M. H.; Liu, X. G. Simultaneous phase and size control of upconversion nanocrystals through lanthanide doping. *Nature* **2010**, *463*, 1061–1065.

[9] Gur, I.; Fromer, N. A.; Geier, M. L.; Alivisatos, A. P. Air-stable all-inorganic nanocrystal solar cells processed from solution. *Science* **2005**, *310*, 462–465.

[10] Fan, Y.; Wang, P. Y.; Lu, Y. Q.; Wang, R.; Zhou, L.; Zheng, X. L.; Li, X. M.; Piper, J. A.; Zhang, F. Lifetime-engineered NIR-II nanoparticles unlock multiplexed *in vivo* imaging. *Nat. Nanotechnol.* **2018**, *13*, 941–946.

[11] Lu, Y. Q.; Zhao, J. B.; Zhang, R.; Liu, Y. J.; Liu, D. M.; Goldys, E. M.; Yang, X. S.; Xi, P.; Sunna, A.; Lu, J. et al. Tunable lifetime multiplexing using luminescent nanocrystals. *Nat. Photonics* **2014**, *8*, 32–36.

[12] Liu, Y. J.; Lu, Y. Q.; Yang, X. S.; Zheng, X. L.; Wen, S. H.; Wang, F.; Vidal, X.; Zhao, J. B.; Liu, D. M.; Zhou, Z. G. et al. Amplified stimulated emission in upconversion nanoparticles for super-resolution nanoscopy. *Nature* **2017**, *543*, 229–233.

[13] Zhan, Q. Q.; Liu, H. C.; Wang, B. J.; Wu, Q. S.; Pu, R.; Zhou, C.; Huang, B. R.; Peng, X. Y.; Ågren, H.; He, S. L. Achieving high-efficiency emission depletion nanoscopy by employing cross relaxation in upconversion nanoparticles. *Nat. Commun.* **2017**, *8*, 1058.

[14] Kostyuk, A. B.; Vorotnov, A. D.; Ivanov, A. V.; Volovetskiy, A. B.; Kruglov, A. V.; Sencha, L. M.; Liang, L. E.; Guryev, E. L.; Vodeneev, V. A.; Deyev, S. M. et al. Resolution and contrast enhancement of laser-scanning multiphoton microscopy using thulium-doped upconversion nanoparticles. *Nano Res.* **2019**, *12*, 2933–2940.

[15] Chen, S.; Weitemier, A. Z.; Zeng, X.; He, L. M.; Wang, X. Y.; Tao, Y. Q.; Huang, A. J. Y.; Hashimotodani, Y.; Kano, M.; Iwasaki, H. et al. Near-infrared deep brain stimulation via upconversion nanoparticle–mediated optogenetics. *Science* **2018**, *359*, 679–684.

[16] Fernandez-Bravo, A.; Yao, K. Y.; Barnard, E. S.; Borys, N. J.; Levy, E. S.; Tian, B. N.; Tajon, C. A.; Moretti, L.; Altoe, M. V.; Aloni, S. et al. Continuous-wave upconverting nanoparticle microlasers. *Nat. Nanotechnol.* **2018**, *13*, 572–577.

[17] Chen, X.; Jin, L. M.; Kong, W.; Sun, T. Y.; Zhang, W. F.; Liu, X. H.; Fan, J.; Yu, S. F.; Wang, F. Confining energy migration in upconversion nanoparticles towards deep ultraviolet lasing. *Nat. Commun.* **2016**, *7*, 10304.

[18] Guo, Q. Y.; Wu, J. H.; Yang, Y. Q.; Liu, X. P.; Jia, J. B.; Dong, J.; Lan, Z.; Lin, J. M.; Huang, M. L.; Wei, Y. L. et al. High performance perovskite solar cells based on β-$NaYF_4$: Yb^{3+}/Er^{3+}/Sc^{3+}@$NaYF_4$ core-shell upconversion nanoparticles. *J. Power Sources* **2019**, *426*, 178–187.

[19] Zhong, Y. T.; Ma, Z. R.; Zhu, S. J.; Yue, J. Y.; Zhang, M. X.; Antaris, A. L.; Yuan, J.; Cui, R.; Wan, H.; Zhou, Y. et al. Boosting the down-shifting luminescence of rare-earth nanocrystals for biological imaging beyond 1,500 nm. *Nat. Commun.* **2017**, *8*, 737.

[20] Zhang, H. X.; Fan, Y.; Pei, P.; Sun, C. X.; Lu, L. F.; Zhang, F. Tm^{3+}-sensitized NIR-II fluorescent nanocrystals for *in vivo* information storage and decoding. *Angew. Chem., Int. Ed.* **2019**, *58*, 10153–10157.

[21] Zhong, Y. T.; Ma, Z. R.; Wang, F. F.; Wang, X.; Yang, Y. J.; Liu, Y. L.; Zhao, X.; Li, J. C.; Du, H. T.; Zhang, M. X. et al. *In vivo* molecular imaging for immunotherapy using ultra-bright near-infrared-IIb rare-earth nanoparticles. *Nat. Biotechnol.* **2019**, *37*, 1322–1331.

[22] Liu, L.; Wang, S. F.; Zhao, B. Z.; Pei, P.; Fan, Y.; Li, X. M.; Zhang, F. Er^{3+} sensitized 1,530 nm to 1,180 nm second near-infrared window upconversion nanocrystals for *in vivo* biosensing. *Angew. Chem., Int. Ed.* **2018**, *57*, 7518–7522.

[23] Lei, X. L.; Li, R. F.; Tu, D. T.; Shang, X. Y.; Liu, Y.; You, W. W.; Sun, C. X.; Zhang, F.; Chen, X. Y. Intense near-infrared-II luminescence from $NaCeF_4$: Er/Yb nanoprobes for *in vitro* bioassay and *in vivo* bioimaging. *Chem. Sci.* **2018**, *9*, 4682–4688.

[24] Wang, F.; Liu, X. G. Upconversion multicolor fine-tuning: Visible to near-infrared emission from lanthanide-doped $NaYF_4$ nanoparticles. *J. Am. Chem. Soc.* **2008**, *130*, 5642–5643.

[25] Wang, Y. F.; Liu, G. Y.; Sun, L. D.; Xiao, J. W.; Zhou, J. C.; Yan, C. H. Nd^{3+}-sensitized upconversion nanophosphors: Efficient *in vivo* bioimaging probes with minimized heating effect. *ACS Nano* **2013**, *7*, 7200–7206.

[26] Shen, J.; Chen, G. Y.; Vu, A. M.; Fan, W.; Bilsel, O. S.; Chang, C. C.; Han, G. Engineering the upconversion nanoparticle excitation wavelength: Cascade sensitization of tri-doped upconversion colloidal nanoparticles at 800 nm. *Adv. Opt. Mater.* **2013**, *1*, 644–650.

[27] Johnson, N. J. J.; He, S.; Diao, S.; Chan, E. M.; Dai, H. J.; Almutairi, A. Direct evidence for coupled surface and concentration quenching dynamics in lanthanide-doped nanocrystals. *J. Am. Chem. Soc.* **2017**, *139*, 3275–3282.

[28] Chen, Q. S.; Xie, X. J.; Huang, B. L.; Liang, L. L.; Han, S. Y.; Yi, Z. G.; Wang, Y.; Li, Y.; Fan, D. Y.; Huang, L. et al. Confining excitation energy in Er^{3+}-sensitized upconversion nanocrystals through Tm^{3+}-mediated transient energy trapping. *Angew. Chem., Int. Ed.* **2017**, *56*, 7605–7609.

[29] Zuo, J.; Li, Q. Q.; Xue, B.; Li, C. X.; Chang, Y. L.; Zhang, Y. L.; Liu, X. M.; Tu, L. P.; Zhang, H.; Kong, X. G. Employing shells to eliminate concentration quenching in photonic upconversion nanostructure. *Nanoscale* **2017**, *9*, 7941–7946.

[30] Savchuk, O. A.; Carvajal, J. J.; Brites, C. D. S.; Carlos, L. D.; Aguilo, M.; Diaz, F. Upconversion thermometry: A new tool to measure the thermal resistance of nanoparticles. *Nanoscale* **2018**, *10*, 6602–6610.

[31] Zhang, H. X.; Jia, T. Q.; Chen, L.; Zhang, Y. C.; Zhang, S.; Feng, D. H.; Sun, Z. R.; Qiu, J. R. Depleted upconversion luminescence in $NaYF_4$: Yb^{3+}, Tm^{3+} nanoparticles via simultaneous two-wavelength excitation. *Phys. Chem. Chem. Phys.* **2017**, *19*, 17756–17764.

[32] Zhang, M. R.; Zheng, W.; Liu, Y.; Huang, P.; Gong, Z. L.; Wei, J. J.; Gao, Y.; Zhou, S. Y.; Li, X. J.; Chen, X. Y. A new class of blue-LED-excitable NIR-II luminescent nanoprobes based on lanthanide-doped CaS nanoparticles. *Angew. Chem., Int. Ed.* **2019**, *58*, 9556–9560.

[33] Sun, T. Y.; Chen, X.; Jin, L. M.; Li, H. W.; Chen, B.; Fan, B.; Moine, B.; Qiao, X.; Fan, X. P.; Tsang, S. W. et al. Broadband Ce(III)-sensitized quantum cutting in core-shell nanoparticles: Mechanistic investigation and photovoltaic application. *J. Phys. Chem. Lett.* **2017**, *8*, 5099–5104.

[34] Zuo, J.; Tu, L. P.; Li, Q. Q.; Feng, Y. S.; Que, I.; Zhang, Y. L.; Liu, X. M.; Xue, B.; Cruz, L. J.; Chang, Y. L. et al. Near infrared light sensitive ultraviolet-blue nanophotoswitch for imaging-guided "Off-On" therapy. *ACS Nano* **2018**, *12*, 3217–3225.

[35] Cheng, X. W.; Pan, Y.; Yuan, Z.; Wang, X. W.; Su, W. H.; Yin, L. S.; Xie, X. J.; Huang, L. Er^{3+} sensitized photon upconversion nanocrystals. *Adv. Funct. Mater.* **2018**, *28*, 1800208.

[36] Zou, W. Q.; Visser, C.; Maduro, J. A.; Pshenichnikov, M. S.; Hummelen, J. C. Broadband dye-sensitized upconversion of near-infrared light. *Nat. Photonics* **2012**, *6*, 560–564.

[37] Xue, B.; Wang, D.; Tu, L. P.; Sun, D. P.; Jing, P. T.; Chang, Y. L.; Zhang, Y. L.; Liu, X. M.; Zuo, J.; Song, J. et al. Ultrastrong absorption meets ultraweak absorption: Unraveling the energy-dissipative routes for dye-sensitized upconversion luminescence. *J. Phys. Chem. Lett.* **2018**, *9*, 4625–4631.

[38] Wang, X. D.; Valiev, R. R.; Ohulchanskyy, T. Y.; Ågren, H.; Yang, C. H.; Chen, G. Y. Dye-sensitized lanthanide-doped upconversion nanoparticles. *Chem. Soc. Rev.* **2017**, *46*, 4150–4167.

[39] Zhou, D. L.; Sun, R.; Xu, W.; Ding, N.; Li, D. Y.; Chen, X.; Pan, G. C.; Bai, X.; Song, H. W. Impact of host composition, codoping, or tridoping on quantum-cutting emission of ytterbium in halide perovskite quantum dots and solar cell applications. *Nano Lett.* **2019**, *19*, 6904–6913.

[40] Swabeck, J. K.; Fischer, S.; Bronstein, N. D.; Alivisatos, A. P. Broadband sensitization of lanthanide emission with indium phosphide quantum dots for visible to near-infrared downshifting. *J. Am. Chem. Soc.* **2018**, *140*, 9120–9126.

[41] Song, D.; Chi, S. Y.; Li, X.; Wang, C. X.; Li, Z.; Liu, Z. H. Upconversion system with quantum dots as sensitizer: Improved photoluminescence and PDT efficiency. *ACS Appl. Mater. Interfaces* **2019**, *11*, 41100–41108.

[42] Garfield, D. J.; Borys, N. J.; Hamed, S. M.; Torquato, N. A.; Tajon, C. A.; Tian, B. N.; Shevitski, B.; Barnard, E. S.; Suh, Y. D.; Aloni, S. et al. Enrichment of molecular antenna triplets amplifies upconverting nanoparticle emission. *Nat. Photonics* **2018**, *12*, 402–407.

[43] Zhang, H. X.; Jia, T. Q.; Shang, X. Y.; Zhang, S. A.; Sun, Z. R.; Qiu, J. R. Mechanisms of the blue emission of $NaYF_4$:Tm^{3+} nanoparticles excited by an 800 nm continuous wave laser. *Phys. Chem. Chem. Phys.* **2016**, *18*, 25905–25914.

[44] Zuo, J.; Sun, D. P.; Tu, L. P.; Wu, Y. N.; Cao, Y. H.; Xue, B.; Zhang, Y. L.; Chang, Y. L.; Liu, X. M.; Kong, X. G. et al. Precisely tailoring upconversion dynamics via energy migration in core-shell nanostructures. *Angew. Chem., Int. Ed.* **2018**, *57*, 3054–3058.

[45] Yan, L.; Zhou, B.; Song, N.; Liu, X. L.; Huang, J. S.; Wang, T.; Tao, L. L.; Zhang, Q. Y. Self-sensitization induced upconversion of Er^{3+} in core- shell nanoparticles. *Nanoscale* **2018**, *10*, 17949–17957.

[46] Sun, T. Y.; Li, Y. H.; Ho, W. L.; Zhu, Q.; Chen, X.; Jin, L. M.; Zhu, H. M.; Huang, B. L.; Lin, J.; Little, B. E. et al. Integrating temporal and spatial control of electronic transitions for bright multiphoton upconversion. *Nat. Commun.* **2019**, *10*, 1811.

[47] Xie, X. J.; Gao, N. Y.; Deng, R. R.; Sun, Q.; Xu, Q. H.; Liu, X. G. Mechanistic investigation of photon upconversion in Nd^{3+}-sensitized core-shell nanoparticles. *J. Am. Chem. Soc.* **2013**, *135*, 12608–12611.

[48] Wen, S. H.; Zhou, J. J.; Schuck, P. J.; Suh, Y. D.; Schmidt, T. W.; Jin, D. Y. Future and challenges for hybrid upconversion nanosystems. *Nat. Photonics* **2019**, *13*, 828–838.

[49] Liang, L. L.; Qin, X.; Zheng, K. Z.; Liu, X. G. Energy flux manipulation in upconversion nanosystems. *Acc. Chem. Res.* **2019**, *52*, 228–236.

[50] Chen, G. Y.; Shao, W.; Valiev, R. R.; Ohulchanskyy, T. Y.; He, G. S.; Ågren, H.; Prasad, P. N. Efficient broadband upconversion of near-infrared light in dye-sensitized core/shell nanocrystals. *Adv. Opt. Mater.* **2016**, *4*, 1760–1766.

[51] Zhao, J. B.; Jin, D. Y.; Schartner, E. P.; Lu, Y. Q.; Liu, Y. J.; Zvyagin, A. V.; Zhang, L. X.; Dawes, J. M.; Xi, P.; Piper, J. A. et al. Single-nanocrystal sensitivity achieved by enhanced upconversion luminescence. *Nat. Nanotechnol.* **2013**, *8*, 729–734.

[52] Gu, Y. Y.; Guo, Z. Y.; Yuan, W.; Kong, M. Y.; Liu, Y. L.; Liu, Y. T.; Gao, Y. L.; Feng, W.; Wang, F.; Zhou, J. J. et al. High-sensitivity imaging of time-domain near-infrared light transducer. *Nat. Photonics* **2019**, *13*, 525–531.

[53] Chan, E. M. Combinatorial approaches for developing upconverting nanomaterials: High-throughput screening, modeling, and applications. *Chem. Soc. Rev.* **2015**, *44*, 1653–1679.

[54] Levy, E. S.; Tajon, C. A.; Bischof, T. S.; Iafrati, J.; Fernandez-Bravo, A.; Garfield, D. J.; Chamanzar, M.; Maharbiz, M. M.; Sohal, V. S.; Schuck, P. J. et al. Energy-looping nanoparticles: Harnessing excited-state absorption for deep-tissue imaging. *ACS Nano* **2016**, *10*, 8423–8433.

[55] Chen, C. C.; Wang, F.; Wen, S. H.; Su, Q. P.; Wu, M. C. L.; Liu, Y. T.; Wang, B. M.; Li, D.; Shan, X. C.; Kianinia, M. et al. Multi-photon near-infrared emission saturation nanoscopy using upconversion nanoparticles. *Nat. Commun.* **2018**, *9*, 3290.

[56] Lei, L.; Xia, H.; Lim, C. K.; Xu, S. Q.; Wang, K.; Du, Y. P.; Prasad, P. N. Modulation of surface energy transfer cascade for reversible photoluminescence pH sensing. *Chem. Mater.* **2019**, *31*, 8121–8128.

[57] Kim, S. Y.; Woo, K.; Lim, K.; Lee, K.; Jang, H. S. Highly bright multicolor tunable ultrasmall β-Na(Y, Gd)F_4: Ce, Tb, Eu/β-$NaYF_4$ core/shell nanocrystals. *Nanoscale* **2013**, *5*, 9255–9263.

[58] Zhou, B.; Tao, L. L.; Chai, Y.; Lau, S. P.; Zhang, Q. Y.; Tsang, Y. H. Constructing interfacial energy transfer for photon up- and down-conversion from lanthanides in a core-shell nanostructure. *Angew. Chem., Int. Ed.* **2016**, *55*, 12356–12360.

[59] Chen, X.; Jin, L. M.; Sun, T. Y.; Kong, W.; Yu, S. F.; Wang, F. Energy migration upconversion in Ce(III)-doped heterogeneous core-shell-shell nanoparticles. *Small* **2017**, *13*, 1701479.

[60] Chen, G. Y.; Damasco, J.; Qiu, H. L.; Shao, W.; Ohulchanskyy, T. Y.; Valiev, R. R.; Wu, X.; Han, G.; Wang, Y.; Yang, C. H. et al. Energy-cascaded upconversion in an organic dye-sensitized core/shell fluoride nanocrystal. *Nano Lett.* **2015**, *15*, 7400–7407.

[61] Wang, D.; Wang, D. P.; Kuzmin, A.; Pliss, A.; Shao, W.; Xia, J.; Qu, J. L.; Prasad, P. N. ICG-sensitized NaYF4: Er nanostructure for theranostics. *Adv. Opt. Mater.* **2018**, *6*, 1701142.

[62] Xu, J. T.; Gulzar, A.; Liu, Y. H.; Bi, H. T.; Gai, S. L.; Liu, B.; Yang, D.; He, F.; Yang, P. P. Integration of IR-808 sensitized upconversion nanostructure and MoS_2 nanosheet for 808 nm NIR light triggered phototherapy and bioimaging. *Small* **2017**, *13*, 1701841.

[63] Hazra, C.; Ullah, S.; Serge Correales, Y. E.; Caetano, L. G.; Ribeiro, S. J. L. Enhanced NIR-I emission from water-dispersible NIR-II dye-sensitized core/active shell upconverting nanoparticles. *J. Mater. Chem. C* **2018**, *6*, 4777–4785.

[64] Li, B. H.; Lu, L. F.; Zhao, M. Y.; Lei, Z. H.; Zhang, F. An efficient 1,064 nm NIR-II excitation fluorescent molecular dye for deep- tissue high-resolution dynamic bioimaging. *Angew. Chem., Int. Ed.* **2018**, *57*, 7483–7487.

[65] Hong, G. S.; Antaris, A. L.; Dai, H. J. Near-infrared fluorophores for biomedical imaging. *Nat. Biomed. Eng.* **2017**, *1*, 0010.

[66] Zheng, W.; Huang, P.; Gong, Z. L.; Tu, D. T.; Xu, J.; Zou, Q. L.; Li, R. F.; You, W. W.; Bünzli, J. C. G.; Chen, X. Y. Near-infrared-triggered photon upconversion tuning in all-inorganic cesium lead halide perovskite quantum dots. *Nat. Commun.* **2018**, *9*, 3462.

[67] Franke, D.; Harris, D. K.; Chen, O.; Bruns, O. T.; Carr, J. A.; Wilson, M. W.; Bawendi, M. G. Continuous injection synthesis of indium arsenide quantum dots emissive in the short-wavelength infrared. *Nat. Commun.* **2016**, *7*, 12749.

[68] Klik, M. A. J.; Gregorkiewicz, T.; Bradley, I. V.; Wells, J. P. R. Optically induced deexcitation of rare-earth ions in a semiconductor matrix. *Phys. Rev. Lett.* **2002**, *89*, 227401.

[69] Martín-Rodríguez, R.; Geitenbeek, R.; Meijerink, A. Incorporation and luminescence of Yb^{3+} in CdSe nanocrystals. *J. Am. Chem. Soc.* **2013**, *135*, 13668–13671.

[70] Zhou, D. L.; Liu, D. L.; Pan, G. C.; Chen, X.; Li, D. Y.; Xu, W.; Bai,

X.; Song, H. W. Cerium and ytterbium codoped halide perovskite quantum dots: A novel and efficient downconverter for improving the performance of silicon solar cells. *Adv. Mater.* **2017**, *29*, 1704149.

[71] Milstein, T. J.; Kroupa, D. M.; Gamelin, D. R. Picosecond quantum cutting generates photoluminescence quantum yields over 100% in ytterbium-doped $CsPbCl_3$ nanocrystals. *Nano Lett.* **2018**, *18*, 3792–3799.

[72] Zhou, J. J.; Deng, J. Y.; Zhu, H. M.; Chen, X. Y.; Teng, Y.; Jia, H.; Xu, S. Q.; Qiu, J. R. Up-conversion luminescence in LaF_3: Ho^{3+} via two-wavelength excitation for use in solar cells. *J. Mater. Chem. C* **2013**, *1*, 8023–8027.

[73] Li, X. M.; Guo, Z. Z.; Zhao, T. C.; Lu, Y.; Zhou, L.; Zhao, D. Y.; Zhang, F. Filtration shell mediated power density independent orthogonal excitations-emissions upconversion luminescence. *Angew. Chem., Int. Ed.* **2016**, *55*, 2464–2469.

[74] You, W. W.; Tu, D. T.; Li, R. F.; Zheng, W.; Chen, X. Y. "Chameleon-like" optical behavior of lanthanide-doped fluoride nanoplates for multilevel anti-counterfeiting applications. *Nano Res.* **2019**, *12*, 1417–1422.

[75] Wang, Y.; Zheng, K. Z.; Song, S. Y.; Fan, D. Y.; Zhang, H. J.; Liu, X. G. Remote manipulation of upconversion luminescence. *Chem. Soc. Rev.* **2018**, *47*, 6473–6485.

[76] Yin, X. M.; Wang, H.; Tian, Y.; Xing, M. M.; Fu, Y.; Luo, X. X. Three primary color emissions from single multilayered nanocrystals. *Nanoscale* **2018**, *10*, 9673–9678.

[77] Wen, S. H.; Zhou, J. J.; Zheng, K. Z.; Bednarkiewicz, A.; Liu, X. G.; Jin, D. Y. Advances in highly doped upconversion nanoparticles. *Nat. Commun.* **2018**, *9*, 2415.

[78] Dai, Y. L.; Xiao, H. H.; Liu, J. H.; Yuan, Q. H.; Ma, P. A.; Yang, D. M.; Li, C. X.; Cheng, Z. Y.; Hou, Z. Y.; Yang, P. P. et al. *In vivo* multimodality imaging and cancer therapy by near-infrared light-triggered trans-platinum pro-drug-conjugated upconverison nanoparticles. *J. Am. Chem. Soc.* **2013**, *135*, 18920–18929.

[79] Zhang, H.; Li, Y. J.; Lin, Y. C.; Huang, Y.; Duan, X. F. Composition tuning the upconversion emission in $NaYF_4$: Yb/Tm hexaplate nanocrystals. *Nanoscale* **2011**, *3*, 963–966.

[80] Liu, G. K. Advances in the theoretical understanding of photon upconversion in rare-earth activated nanophosphors. *Chem. Soc. Rev.* **2015**, *44*, 1635–1652.

[81] Yang, D. M.; Ma, P. A.; Hou, Z. Y.; Cheng, Z. Y.; Li, C. X.; Lin, J. Current advances in lanthanide ion (Ln^{3+})-based upconversion nanomaterials for drug delivery. *Chem. Soc. Rev.* **2015**, *44*, 1416–1448.

[82] Gai, S. L.; Li, C. X.; Yang, P. P.; Lin, J. Recent progress in rare earth micro/nanocrystals: Soft chemical synthesis, luminescent properties, and biomedical applications. *Chem. Rev.* **2014**, *114*, 2343–2389.

[83] Zhan, Q. Q.; Qian, J.; Liang, H. J.; Somesfalean, G.; Wang, D.; He, S. L.; Zhang, Z. G.; Andersson-Engels, S. Using 915 nm laser excited Tm^{3+}/Er^{3+}/Ho^{3+}-doped $NaYbF_4$ upconversion nanoparticles for *in vitro* and deeper *in vivo* bioimaging without overheating irradiation. *ACS Nano* **2011**, *5*, 3744–3757.

[84] Zhan, Q. Q.; He, S. L.; Qian, J.; Cheng, H.; Cai, F. H. Optimization of optical excitation of upconversion nanoparticles for rapid microscopy and deeper tissue imaging with higher quantum yield. *Theranostics* **2013**, *3*, 306–316.

[85] Ortgies, D. H.; Tan, M. L.; Ximendes, E. C.; Del Rosal, B.; Hu, J.; Xu, L.; Wang, X. D.; Martí n Rodríguez, E.; Jacinto, C.; Fernandez, N. et al. Lifetime-encoded infrared-emitting nanoparticles for *in vivo* multiplexed imaging. *ACS Nano* **2018**, *12*, 4362–4368.

[86] Cao, C.; Xue, M.; Zhu, X. J.; Yang, P. Y.; Feng, W.; Li, F. Y. Energy transfer highway in Nd^{3+}-sensitized nanoparticles for efficient near-infrared bioimaging. *ACS Appl. Mater. Interfaces* **2017**, *9*, 18540–18548.

[87] Petit, V.; Camy, P.; Doualan, J. L.; Moncorgé, R. CW and tunable laser operation of Yb^{3+} in Nd: Yb: CaF_2. *Appl. Phys. Lett.* **2006**, *88*, 051111.

[88] Liu, Y. X; Wang, D. S.; Shi, J. X.; Peng, Q.; Li, Y. D. Magnetic tuning of upconversion luminescence in lanthanide-doped bifunctional nanocrystals. *Angew. Chem., Int. Ed.* **2013**, *52*, 4366–4369.

[89] Zhou, J. J.; Shirahata, N.; Sun, H. T.; Ghosh, B.; Ogawara, M.; Teng, Y.; Zhou, S. F.; Chu, R. G. S.; Fujii, M.; Qiu, J. R. Efficient dual-modal NIR-to-NIR emission of rare earth ions co-doped nanocrystals for biological fluorescence imaging. *J. Phys. Chem. Lett.* **2013**, *4*, 402–408.

[90] Deng, R. R.; Qin, F.; Chen, R. F.; Huang, W.; Hong, M. H.; Liu, X. G. Temporal full-colour tuning through non-steady-state upconversion. *Nat. Nanotechnol.* **2015**, *10*, 237–242.

[91] He, F.; Yang, G. X.; Yang, P. P.; Yu, Y. X.; Lv, R. C.; Li, C. X.; Dai, Y. L.; Gai, S. L.; Lin, J. A new single 808 nm NIR light-induced imaging-guided multifunctional cancer therapy platform. *Adv. Funct. Mater.* **2015**, *25*, 3966–3976.

[92] Ding, X.; Liu, J. H.; Liu, D. P.; Li, J. Q.; Wang, F.; Li, L. J.; Wang, Y. H.; Song, S. Y.; Zhang, H. J. Multifunctional core/satellite polydopamine@Nd^{3+}-sensitized upconversion nanocomposite: A single 808 nm near-infrared light-triggered theranostic platform for *in vivo* imaging-guided photothermal therapy. *Nano Res.* **2017**, *10*, 3434–3446.

[93] Wang, H.; Liu, Y.; Wang, Z. H.; Yang, M.; Gu, Y. Q. 808 nm-light-excited upconversion nanoprobe based on LRET for the ratiometric detection of nitric oxide in living cancer cells. *Nanoscale* **2018**, *10*, 10641–10649.

[94] Wang, R.; Li, X. M.; Zhou, L.; Zhang, F. Epitaxial seeded growth of rare-earth nanocrystals with efficient 800 nm near-infrared to 1,525 nm short-wavelength infrared downconversion photoluminescence for *in vivo* bioimaging. *Angew. Chem., Int. Ed.* **2014**, *53*, 12086–12090.

[95] Dong, H.; Sun, L. D.; Feng, W.; Gu, Y. Y.; Li, F. Y.; Yan, C. H. Versatile spectral and lifetime multiplexing nanoplatform with excitation orthogonalized upconversion luminescence. *ACS Nano* **2017**, *11*, 3289–3297.

[96] Liu, B.; Li, C. X.; Yang, P. P.; Hou, Z. Y.; Lin, J. 808-nm-light-excited lanthanide-doped nanoparticles: Rational design, luminescence control and theranostic applications. *Adv. Mater.* **2017**, *29*, 1605434.

[97] Cheng, X. W.; Ge, H.; Wei, Y.; Zhang, K.; Su, W. H.; Zhou, J. M.; Yin, L. S.; Zhan, Q. Q.; Jing, S.; Huang, L. Design for brighter photon upconversion emissions via energy level overlap of lanthanide ions. *ACS Nano* **2018**, *12*, 10992–10999.

[98] Xie, S. W.; Gong, G.; Song, Y.; Tan, H. H.; Zhang, C. F.; Li, N.; Zhang, Y. X.; Xu, L. J.; Xu, J. X.; Zheng, J. Design of novel lanthanide-doped core-shell nanocrystals with dual up-conversion and down-conversion luminescence for anti-counterfeiting printing. *Dalton Trans.* **2019**, *48*, 6971–6983.

[99] Hong, G. S.; Diao, S.; Chang, J. L.; Antaris, A. L.; Chen, C. X.; Zhang, B.; Zhao, S.; Atochin, D. N.; Huang, P. L.; Andreasson, K. I. et al. Through-skull fluorescence imaging of the brain in a new near-infrared window. *Nat. Photonics* **2014**, *8*, 723–730.

[100] Antaris, A. L.; Chen, H.; Cheng, K.; Sun, Y.; Hong, G. S.; Qu, C. R.; Diao, S.; Deng, Z. X.; Hu, X. M.; Zhang, B. et al. A small-molecule dye for NIR-II imaging. *Nat. Mater.* **2016**, *15*, 235–242.

[101] Ding, F.; Fan, Y.; Sun, Y.; Zhang, F. Beyond 1,000 nm emission wavelength: Recent advances in organic and inorganic emitters for deep-tissue molecular imaging. *Adv. Healthc. Mater.* **2019**, *8*, 1900260.

[102] Zhang, X. B.; Chen, W. W.; Xie, X. Y.; Li, Y. Y.; Chen, D. S.; Chao, Z. C.; Liu, C. H.; Ma, H. B.; Liu, Y.; Ju, H. X. Boosting luminance energy transfer efficiency in upconversion nanoparticles with an energy-concentrating zone. *Angew. Chem., Int. Ed.* **2019**, *58*, 12117–12122.

[103] Ke, J. X.; Lu, S.; Shang, X. Y.; Liu, Y.; Guo, H. H.; You, W. W.; Li, X. J.; Xu, J.; Li, R. F.; Chen, Z. et al. A strategy of NIR dual-excitation upconversion for ratiometric intracellular detection. *Adv. Sci.* **2019**, *6*, 1901874.

[104] Zou, X. M.; Zhou, X. B.; Cao, C.; Lu, W. Y.; Yuan, W.; Liu, Q.Y.; Feng, W.; Li, F. Y. Dye-sensitized upconversion nanocomposites for ratiometric semi-quantitative detection of hypochlorite *in vivo*. *Nanoscale* **2019**, *11*, 2959–2965.

[105] Zhang, D. L.; Wang, L. L.; Yuan, X.; Gong, Y. J.; Liu, H. W.; Zhang, J.; Zhang, X. B.; Liu, Y. L.; Tan, W. H. Naked-eye readout of analyte-induced NIR fluorescence responses by an initiation-input-transduction nanoplatform. *Angew. Chem., Int. Ed.* **2020**, 59, 695–699.

[106] Liang, T.; Li, Z.; Wang, P. P.; Zhao, F. Z.; Liu, J. Z.; Liu, Z. H. Breaking through the signal-to-background limit of upconversion nanoprobes using a target-modulated sensitizing switch. *J. Am. Chem. Soc.* **2018**, *140*, 14696–14703.

[107] Shao, W.; Chen, G. Y.; Kuzmin, A.; Kutscher, H. L.; Pliss, A.; Ohulchanskyy, T. Y.; Prasad, P. N. Tunable narrow band emissions from dye-sensitized core/shell/shell nanocrystals in the second near-infrared biological window. *J. Am. Chem. Soc.* **2016**, *138*, 16192–16195.

[108] Lee, J.; Yoo, B.; Lee, H.; Cha, G. D.; Lee, H. S.; Cho, Y.; Kim, S. Y.; Seo, H.; Lee, W.; Son, D. et al. Ultra-wideband multi-dye-sensitized upconverting nanoparticles for information security application. *Adv. Mater.* **2017**, *29*, 1603169.

[109] Xu, J. T.; Yang, P. P.; Sun, M. D.; Bi, H. T.; Liu, B.; Yang, D.; Gai, S. L.; He, F.; Lin, J. Highly emissive dye-sensitized upconversion nanostructure for dual-photosensitizer photodynamic therapy and bioimaging. *ACS Nano* **2017**, *11*, 4133–4144.

[110] Mukherjee, P.; Sloan, R. F.; Shade, C. M.; Waldeck, D. H.; Petoud, S. A postsynthetic modification of II-VI semiconductor nanoparticles to create Tb^{3+} and Eu^{3+} luminophores. *J. Phys. Chem. C* **2013**, *117*, 14451–14460.

[111] Chengelis, D. A.; Yingling, A. M.; Badger, P. D.; Shade, C. M.; Petoud, S. Incorporating lanthanide cations with cadmium selenide nanocrystals: A strategy to sensitize and protect Tb(III). *J. Am. Chem. Soc.* **2005**, *127*, 16752–16753.

[112] Creutz, S. E.; Fainblat, R.; Kim, Y.; De Siena, M. C.; Gamelin, D. R. A selective cation exchange strategy for the synthesis of colloidal Yb^{3+}-doped chalcogenide nanocrystals with strong broadband visible absorption and long-lived near-infrared emission. *J. Am. Chemi. Soc.* **2017**, *139*, 11814–11824.

[113] Hu, Q. S.; Li, Z.; Tan, Z. F.; Song, H. B.; Ge, C.; Niu, G. D.; Han, J. T.; Tang, J. Rare earth ion-doped $CsPbBr_3$ nanocrystals. *Adv. Opt. Mater.* **2018**, *6*, 1700864.

[114] Pan, G. C.; Bai, X.; Yang, D. W.; Chen, X.; Jing, P. T.; Qu, S. N.; Zhang, L. J.; Zhou, D. L.; Zhu, J. Y.; Xu, W. et al. Doping lanthanide into perovskite nanocrystals: Highly improved and expanded optical properties. *Nano Lett.* **2017**, *17*, 8005–8011.